Photo Degradation of Organophosphate Pesticides (Acephate & Omethoate) with N-Doped TiO_2 in Presence and Absence of Visible Light

By

Sumaira Shah

School of Chemical and Materials Engineering (SCME)

National University of Sciences and Technology (NUST)

2016

Photo Degradation of Organophosphate Pesticides (Acephate & Omethoate) with N-Doped TiO_2 in Presence and Absence of Visible Light

Name: Sumaira Shah

Reg. No: NUST201362344MSCME67813F

This thesis is submitted as a partial fulfilment of the requirements for the degree of

MS in Chemical Engineering

Supervisor: Dr. Habib Nasir

School of Chemical and Materials Engineering (SCME)

National University of Sciences and Technology (NUST)

H-12 Islamabad, Pakistan

August, 2016

Dedications

Thanks to almighty Allah for giving me the stamina and intellect, thanks to my honorable and ever loving parents for encouraging me in every moment of disappointment. Then thanks to respected teachers and my friends for helping me.

The work is dedicated to my siblings for their good wishes and moral support, especially to my brother Zulfiqar Ali Shah who made my dream possible. It was his patience and love to be with me in any rough situation throughout my MS.

Abstract

Rising demand for the crop production is increasing the use of pesticides and herbicides. Organophosphorous pesticides like acephate and omethoate are the most harmful chemicals and are playing the main role in the water and soil pollution. These are slow biodegradable organic compounds and are contaminating the environment. The increasing awareness for the environmental remediation has made human to investigate novel researches for the photo degradation of such toxic compounds. In the present work nanoparticles of TiO_2 were synthesized by sol gel method using titanium tetraisopropoxide, 2-propanol in distilled water. The nanoparticles so formed were then doped with nitrogen by using urea as nitrogen source. Different ratios of TiO_2 to urea i-e (1:0), (1:0.1), (1:0.5), (1:1), (1:2) and (1:3) were used to synthesize six different types of nanocatalysts. The catalysts were symbolized as SN-0, SN-0.1, SN-0.5, SN-1, SN-2 and SN-3 respective to the ratio of urea used.

These as prepared N-doped catalysts were then characterized with various techniques i-e SEM, EDS, XRD UV-visible spectroscopy and BET. From SEM the spherical morphology of all the catalysts was seen and particle size within nano range was investigated. The EDS showed the elemental composition. Through XRD the anatase phase and tetragonal structure was confirmed and the crystallite sizes were also calculated. From UV-visible spectra band gap was calculated by Tauc plot. From BET analysis the surface area and pore size of each catalyst was found. The photo catalytic activity of all the catalysts was evaluated from the degradation study of acephate and omethoate pesticides. The decrease in concentration was found from UV visible spectrophotometer. As compared to all the synthesized and bulk TiO_2, SN-3 nanocatalyst showed the highest activity due to its smaller crystallite size, lower band gap and larger surface area.

List of Acronyms

AChE (Acetyl cholinesterase)

BET (Brunauer-Emmett-Teller)

EDX (Energy Dispersive X-Ray Spectroscopy)

FTIR (Fourier Transform Infrared Spectroscopy)

Ops (Organophosphates)

SEM (Scanning Electron Microscopy)

TTIP (Titanium tetra isopropoxide)

UV-Vis (Ultra Violet-Visible Spectroscopy)

XRD (X-Ray Diffraction)

Acknowledgements

All praises accolade to the greatest Allah who is the most merciful and exalter; for giving me the intellect and ability to accomplish this research work.

Then I wish to express my sincerest indebtedness to my venerable supervisor **Prof. Dr. Habib Nasir**, for giving me his precious time and providing his kind guidance. He has been the source of inspiration for me and his encouragement and motivations have been of greatest help.

After that I would like to thank my Guidance & Examination Committee members Dr. Arshad Chughtai and Dr. Tayyaba Noor for their counselling, suggestions and enlightment.

Table of Contents

List of Figures

List of Tables

Chapter 1: Introduction

This chapter explains the pesticide, its classifications, importance of pesticides, their impact on human environment, the procedures for environmental remediation, photo catalysis, TiO_2 and the property modifications of TiO_2 by different methods.

Introduction

Pakistan is blessed with vast natural resources, and it is home to various ecological and climatic zones. It has a greater potential for growing all kinds of food commodities. Agriculture affects the generating economic growth both directly and indirectly. The impact of agriculture on our economy is that it is a source of food which is the basic need of human beings and animals. It also gives us fibers for the domestic industries. It is a source of foreign exchange earnings and provides a platform for the industrial business.

Pakistan has the largest number of lands for irrigation in the world. The vast cultivable lands offer good possibilities of crop production increasing the economy of the country [1]. Crop production is threatened by pests, weeds and insects. Pests are living organisms that cause unwanted effects. These pests damage the leaves and fruits of plants, hence hinders the growth of plant.

Figure 1.1 Leaf damaged by pest

1.1. Pesticides

For managing the hazards and damages of the pests, various chemical compounds called as pesticides are introduced. Pesticide is any synthetic or natural chemical compound that kills pests, weeds and insects and thus protects our crops. These pesticides are applied to the plants in different forms like sprays, gas, liquids, dusting, fumigation, fogging (thermal/cold), ultra-low volume spraying, pellets, and powders. All forms are hazardous for environment especially for human health. The pesticide contains one or more active ingredients and some additives. The active ingredients are the chemicals that kill the target pests. And the additives are the ingredients that make the product safer, efficient and convenient to apply [2].

1.1.1. Classification of pesticides

On the basis of chemical composition the pesticides are broadly divided as organic and inorganic pesticides. The organic pesticides are usually not soluble in water and are complex than the inorganic. These are then classified according to the chemical structures. The following are the main types:

- ***Organo Chlorine***

These are chlorinated hydrocarbons, and are very stable. These pesticides were discovered very earlier and were the first to be used for protecting crops. Now their use is prohibited due to their high toxicity. They are very persistent in the environment and are insoluble in water, they cause head ache, nausea, vomiting and weakness. Some examples of these pesticides are dichlorodiphenyltrichloroethane (DDT), methoxychlor, dieldrin, chlordane, and benzene hexachloride.

- ***Carbamates***

These pesticides are basically esters derived from acids or dimethyl N-methyl carbamic acid. They have very low potential for bioaccumulation, thus do not stay for long in the environment. Carbamates are further classified into carbamates, thiocarbamates and dithiocarbamates.

Carbamates enter the human body through skin, inhalation, or ingestion. High doses are toxic and cause nausea, weakness and paralysis.

- ***Pyrethroids***

Carbamates are replaced by pyrethroids, the natural pesticides derived from pyrethrin an extract of chrysanthemum flowers. These are also synthesized nowadays.

Pyrethroids are complex mixtures of chemical isomers, solvent oils, and piperonyl butoxide. They are less volatile, do not bind to soils, and are not soluble in water bodies. They have higher degradation rates and thus do not contaminate in the environment [3].

- ***Organophosphates***

The most widely used pesticides, on the basis of their chemical combination they are esters of phosphoric acid. These pesticides are moderately soluble in water and have low vapor pressure. Toxicity level is high because these pesticides hit the central nervous system; inhibit the acetyl cholinesterase which is an enzyme that controls the neurotransmitter acetylcholine level, destroy the nerve impulse by serine phosphorylation of the hydroxyl group in the active site of the enzyme [3]. Acephate, omethoate, chloropyrifos, endosulphon, imidocloprid, quinolphos etc are the commonly used organophosphorous pesticides.

The current work is about the degradation of two main organophosphorous pesticides i-e acephate and omethoate.

1.1.1.1. Acephate

The organophosphorous pesticide having the IUPAC name as *O*,*S*-Dimethyl *N*-acetylphosphoramidothioate is generally known as acephate. It is a white transparent solid, smells like sulphur. It has the molecular formula of $C_4H_{10}NO_3PS$ and molar mass = 183.165 g/mol.

Acephate does not stay for long in the environment; its degradation rate is about 10 to 15 days. Its solubility in water is 79-83.5 g/100 mL.

After degradation in soil acephate forms methamidophos which is another organophosphorous pesticide. The methamidophos inhibits acetyl cholinesterase through

phosphorylation. The acephate can also be transformed into S-methylacetyl phosphoramidothiolate which is not an acetyl cholinesterase inhibitor. Its exposure causes diarrhea, abdominal cramps, coughing, pneumonia, swelling and rashes [4].

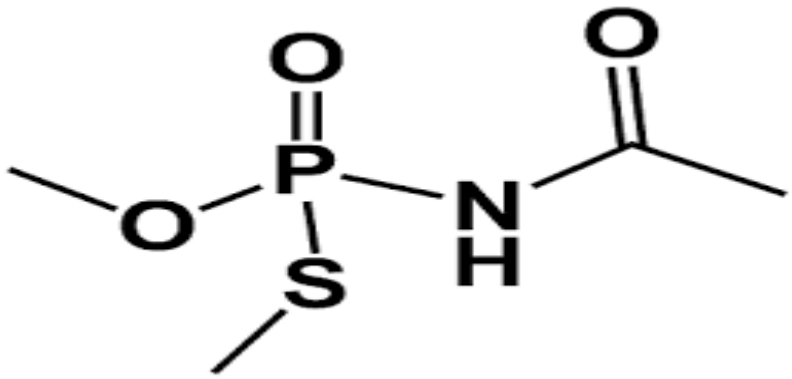

Figure 1.2 Structural formula of acephate [5]

1.1.1.2. Omethoate

Omethoate is white crystalline solid. The IUPAC name of omethoate is 2-(Dimethoxyphosphoryl) sulfanyl-N-methyl-acetamide. Other name is *O,O*-Dimethyl S-methylcarbamoylmethyl phosphorothioate. It has a molar mass of 213.19 g/mol, it is less water miscible, is more soluble in organic solvents like acetone. It is very persistent in the environment and has a half-life of more than 68 days. Upon degradation it is converted to dimethyl hydrogen phosphate and dimethoxon [6].

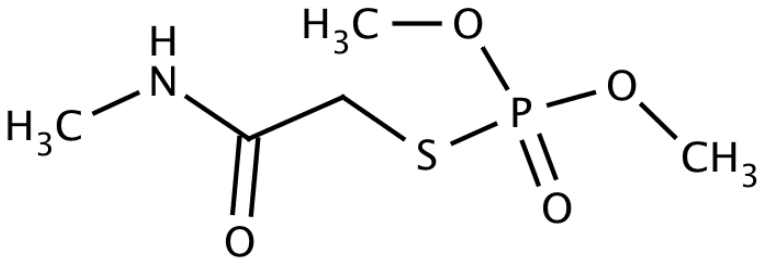

Figure 1.3 Structural formula of omethoate [7]

1.2. Importance of Pesticides

Pakistan is blessed with a land suitable for many crops. About 64 % population depends upon agriculture. With increasing population the demand for vegetables and agro products is emerging day by day. To fulfill this demand and improve land fertility a need for introducing benign fertilizers and pesticides are needed. The pesticides play a vital role in increasing the crop production.

The increasing population along with improvement in dietary habits towards good quality products is raising the demand for more grain production. However the availability of cultivable land is low and the soil with high productivity potential is already under in use. Secondly the availability of water is limited, and in some regions land resources are depleting day by day and the cultivated area is under constant shrinkage [8].

Figure 1.4 Vegetables free of pests [9]

To cope with these limitations, higher production rate is required. Another solution is the fertile land conservation should be achieved. The improvement in high-yielding varieties is the major challenge to this sector. The grown crops then need protection from damages by weeds and pests. These pathogens also need to be overcome for providing enough quantity and high quality food.

To improve the crop management systems on the basis of crop quality, soil fertility through chemical fertilizers, and pest control should be ensured. These

improvement and irrigations are the achievements of the Green Revolution. These factors increased the world food production to past 35 years [10].

Most of the diverse ecosystems are replaced by agro-ecosystems in all regions that are specifically more prone to pest attack. To enhance the crop productivity in order to overcome the rising demand, these crops should be protected from pests. The required high yield of cultivated plants is threatened by destruction from pests [11].

The invention of synthetic insecticides organophosphate insecticides, carbamates pyrethroids, herbicides and fungicides from 1960s through 1980s contributed to a greater extent over the pest control and agricultural output. Pesticides thus play a very important role in the economic growth of a country. They reduce the crop loss which is caused by the plant diseases and insects [12]. With the use of pesticides considerable economic losses can be controlled and without pesticides a significant decrease in yield and economic margin can be quantified. Pesticides thus have a significant role in economic growth [13].

Soil-borne pests and diseases are the major issues with many vegetables. These pests are difficult to detect because of their smaller size, (e.g. fungal pathogens, nematodes) and their life stages that compose of a resting stages and an active stage. Pesticide treatment during the growth of the vegetables is almost impossible. Any control system for detection and diagnosis requires high effort and special devices. Growers generally kill the threat of soil-borne pests and diseases with prophylactic applications of pesticides [12].

1.3. Environmental Impacts of Pesticides

With the invention of pesticide it was apparently thought that these pesticides may be harmful to the pests only and not to the other species like human beings and animals. But the case is not so true; the pesticides are polluting the human environment and are lethal for the human being. The rampant use of pesticides under the adage, “if little works good, a little more will do much better” has ruined the human environment.

Application of pesticide to a target pest (plant or animal) affects the immediate area including crops, soil organism, human beings and wildlife. Some of it goes to the air or to surface waters affecting the aquatic life [12].

1.3.1. Direct effect on human beings

Several chemicals like pesticides are termed as endocrine disruptors because they harm the human directly through inhalation. They affect the hormones that are naturally secreted within the body and their long term exposure is increasingly affecting the human health by suppressing the immune system, hormone disruption, reduced intelligence, liver malfunction, neurologic impairment, and abnormalities in new born babies, cardiovascular problems, diabetes and cancer. These organic chemicals are very toxic in nature [14].

1.3.2. Impact of pesticides on food commodities

Pesticides can harm the human indirectly by contamination in food. A lot of work has been done for the investigation of pesticides contamination in vegetables and fruits, most of the researchers revealed that pesticides like acephate, chlopyriphos, chlopyriphosmethyl, methamidophos, iprodione, procymidone and chlorothalonil tend to contaminate the vegetables especially lettuce leaves, bananas, beans, and potatoes [14].

1.3.3. Contaminating soil and water

Because of the low solubility and resonant ring structures of various organic substances such as polysaccharides, phenolic material, detergents, pesticides and dyes, they are extremely resistant to biodegradation and baffle difficulties in municipal and industrial wastewater treatment. Conventional methods for the treatment of wastewater are not good enough to control the rising level of these toxic compounds in wastewater.

Pesticides persist in the water bodies, soil and pollute the air. They also harm the beneficial microorganisms, insects and also weaken the roots of plants. This contamination depends on the physical and chemical properties of pesticides i-e partition coefficients, rate of degradation, deposition rates and also on the characteristics of the environment [14-15].

Pesticides adhere to fine soil particles and organic matter. They bind to soil particles so that migration of the contaminant is limited. This binding of pesticides depends on the solubility of a pesticide in water. This downward mobility of pesticides can be avoided by the addition of some fertilizers or lowering of soil pH and irrigation[16].

1.4. Environmental remediation

Several methods are being used for the effluent treatment. These include the removal of dyes and heavy metals from water. Physical methods for such treatment include precipitation, adsorption, and reverse osmosis (Mainly water purification); chemically this treatment is done through oxidation (using air oxygen; ozone, NaOC1, and H_2O_2 as oxidants) and reduction (e.g., $Na_2S_2O_4$); and the last method is the biological methods which is classified as aerobic and anaerobic treatment[17]. The drawback of these conventional treatments is the formation of large amount of sludge. The disposal of such sludge raises the operation cost, time consumption and ineffectiveness.

1.4.1. Bioremediation

Temporary treatment of the contaminated soil is the mixing of non-contaminated soil with the contaminated one, removing the upper layer that is contaminated. These methods are temporary and are not efficient.

Bioremediation of pesticides is one of the environmental friendly and economic methods for their detoxification. The factor that affects the biodegradability of pesticides is the characteristics of the chemical compounds [17].

1.4.2. Phytoremediation for pesticides

Another important and economical method for pesticides control is phytoremediation. This method involves the degradation of xenobiotics in the rhizosphere of plants by some enzymes microbial action [18].

1.4.3. Physical methods for pesticides control

To achieve the most efficient control over pesticides and other organic pollutants waste, physical processes of waste water purification like adsorption on activated charcoal and flocculation were used but these methods cannot destroy the pollutant, but can only transform them to other form, so creating secondary pollution [19].

1.4.4. Chemical Methods

Chemical processes involve the degradation of these toxic compounds into harmless or benign compounds by the use of some catalyst in presence of sunlight or ultra violet light.

1.5. Photo catalytic degradation

Catalysts are used for lowering the energy for reaction to enhance the rate of reaction. Catalysis is classified into two main types 1) Heterogeneous catalysis 2) Homogenous catalysis.

Most of the reactions are forced to occur in the presence of sunlight using a catalyst. Such type of reactions is photo catalytic reactions. In this reaction the light is absorbed by the catalyst, the activity of the reaction depends on the catalyst; it involves the photosensitization of the surface of catalyst that generates electron–hole pairs, which then create hydroxyl and superoxide radicals that initiate the reaction with the substrate.

Microbial degradation, mechanochemical destruction, activated carbon adsorption, precipitation and photo catalysis is widely used for the removal of organic pollutant from waste water and soil.

This conventional degradation is nowadays altered by the use of nano catalysis. By reducing the particle size to nanoscale the properties of that material can be enhanced especially catalytic properties. This property modification is due to the increase in the surface area, which expose a large number of active sites. Playing with the size, shape and morphology of nanoparticles the activities of particles can be manipulated. Transition metals, non-metals and metal oxides are used as catalysts. These catalysts are

found to be efficient for most of the reactions and some of them are inexpensive and available everywhere. Metal oxide catalysts have attracted more attention due to their high chemical selectivity, metallic nature and semiconductor qualities.

Metal oxide catalysts have the oxide as the active phase and some additive are used as matrix for it [20].

1.6. Catalytic properties of TiO_2

Titanium dioxide (TiO_2) is a white, opaque pigment with high refractive index[21].It is the most widely used photo catalyst. Its extensive use is attributed to its thermal and chemical stability, high oxidation reduction potential, dielectric properties, strong adsorption capacity, nontoxicity, and inexpensive properties[22]. The surface of TiO_2 has both the Lewis acid and Lewis base character that make it an excellent adsorbent for many organic pollutants [20].

With the exposure of UV light holes and electrons are generated on the surface of TiO_2, the holes have the highest oxidizing potential to oxidize almost all the toxic compounds to CO_2. The electrons tend to reduce the oxygen; this phenomenon has made TiO_2 the superior photo catalyst. Another feature of TiO_2 is that its surface is super hydrophilic, with a contact angle of 0^o [23].

TiO_2 has vast applications in self-cleaning tiles, antifogging mirrors, air cleaners, and odor removal [22].

TiO_2has three morphological forms; 1) brookite/amorphous form 2) Rutile and 3) anatase phase.

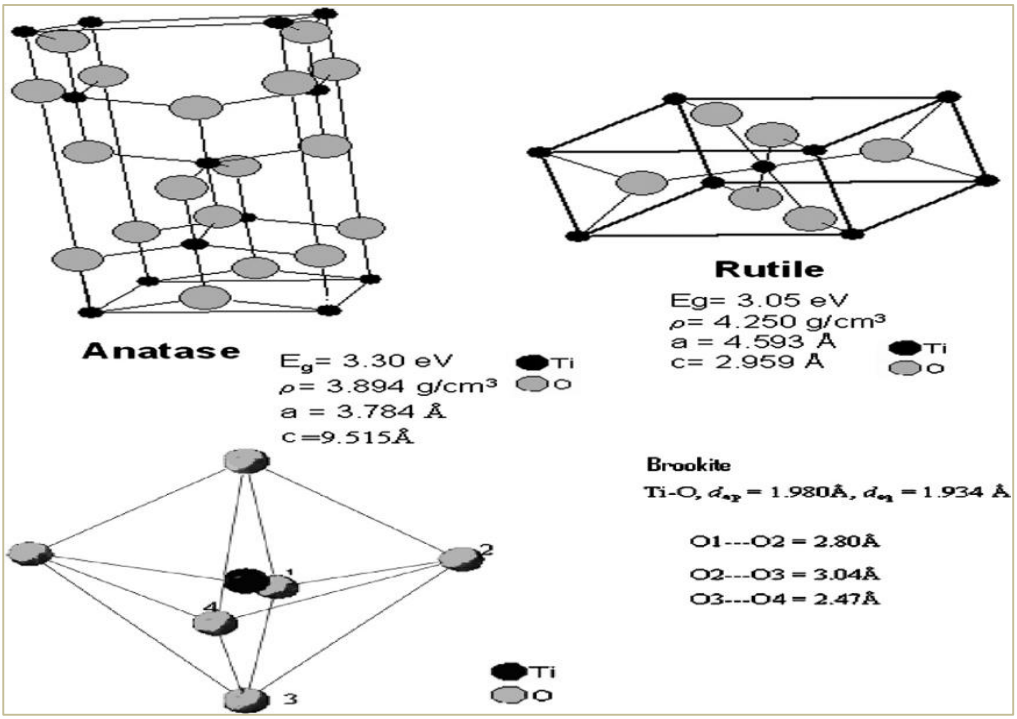

Figure 1.5 Morphological forms of Titania [24]

TiO_2 has an octahedral structure, the rutile phase shares corner and edges with eight and two neighbors respectively, thus forms a linear form. Rutile phase is the most stable phase[25]. This phase has a smaller metal-metal distance and larger band gap of 3.0 eV.

In the anatase the octahedron shares edges and corners with four atoms, thus gives a zig zag chain. The band gap of anatase is 3.2 eV [23].

The photo catalytic activity of the TiO_2depends on:

(i) Light absorption
(ii) The electron or hole-induced redox reaction rate
(iii) The electron-hole recombination

The catalytic activity of TiO_2 under visible light is limited by its larger band gap and higher electron hole recombination rate.

The electron-hole recombination rate is affected by the size, surface area and crystallinity of the catalyst[26].

By increasing the surface to volume ratio, optimizing particle size, making composite or doping of metals and non-metals the catalytic activity of TiO_2 can be modified [27].

Due to the larger band gap only a small portion i-e 4% of the sunlight can be utilized. To make it active in visible light some metals and non-metals is to be doped with the TiO_2. Nonmetals i-e N, S, F, C and I doping significantly narrow the band gap of TiO_2 and give a red shift up to 540 nm [22].

In the current work TiO_2 is to be doped with Nitrogen to get a photo catalytic response in the visible region.

Nitrogen is an anionic dopant, and is more efficient because of the atomic size comparable to that of oxygen, smaller ionization energy, meta stable center formation and chemical stability [23].

1.7 Objectives of the project

- Synthesis of TiO_2 nanoparticles
- Doping the prepared nanocatalyst with different percentage of Nitrogen
- Characterization of N-doped TiO_2 by different techniques
- Photo catalytic activity evaluation of these catalysts by the degradation of organophosphorous pesticides (acephate and omethoate)

Chapter 2: Literature survey

This chapter is a review of the previous work reported in the literature relevant to the mentioned work. The chapter is divided into five section, 2.1 is discussion on general photo catalysis, 2.2 is about catalytic activity of TiO_2, 2.3 explains all the previous work done for the modification of the photo activity of TiO_2 by doping Nitrogen and formation of nano composite, the degradation of organophosphorous pesticides is described in the last section.

2.1. Photo catalysis

Photo catalysis is the process which accelerates by the interaction of a material (catalyst) with light of certain wavelength. When a ray of light having energy more than the band gap of the catalyst is illuminated, generation of active oxidizing and reducing species i-e holes and electrons occurs. The holes are created in the valence band while the electrons are excited in the conduction band, the holes transform the substrate i-e pollutant into other form and electrons reduce the oxygen. The phenomenon of photo catalysis occurs by the oxidation of water and reduction of an electron acceptor by the electrons that are excited by the light energy. The hydroxyl and superoxide radical anion is created. The following is the reaction that occurs during the whole process [23].

$$\text{Catalyst} + \text{photon} \rightarrow \text{holes}^{+}_{VB} + \text{electrons}^{-}_{CB}$$

$$\text{electrons}^{-}_{CB} + \text{holes}^{+}_{VB} \rightarrow \text{energy}$$

$$H_2O + \text{holes}^{+}_{VB} \rightarrow {}^{\bullet}OH + H^{+}$$

$$O_2 + \text{electrons}^{-}_{CB} \rightarrow O_2^{\bullet-}$$

$${}^{\bullet}OH + \text{substrate} \rightarrow H_2O + CO_2$$

$$O_2^{\bullet-} + H^{+} \rightarrow {}^{\bullet}OOH$$

$${}^{\bullet}OOH + {}^{\bullet}OOH \rightarrow H_2O_2 + O_2$$

$$O_2^{\bullet-} + \text{substrate} \rightarrow CO_2 + H_2O$$

$${}^{\bullet}OOH + \text{substrate} \rightarrow CO_2 + H_2O \quad [25]$$

Photo catalytic oxidation is a cost-effective, highly efficient and environmentally benign technology for treating low concentration pollutants at low temperature and pressure. The oxidation products of most organic pollutants are carbon dioxide and water.

Akira Fujishima1960 discovered the rutile phase of TiO_2. He found it a transparent glass like crystal, highly stable in electrolytic solution. He worked on an electrochemical circuit to investigate the oxidation potential of TiO_2. The $TiO_2$was used as an electrode with the platinum black. A current flow occurred when the TiO_2electrode was illuminated with light of wavelength λ=415 nm. From this experiment he suggested that water can be decomposed under UV-visible light without applying any voltage. This investigation suggested a clean source of energy production and gave a path to extend the photo splitting to photo catalysis [22].

Lixin Cao, Aimin Huang et al., 1999 investigated the gas-phase degradation of 1-butene by using nanoscale TiO_2 as photo catalyst. The catalyst was synthesized by the acid-assisted sol–gel method. The photo activity of catalyst was affected by the synthesis procedures followed, humidity, and calcination temperatures. Calcination temperature about 300°C resisted the catalysts poisoning and temperature up to 400°C lowered the photo activity because of the phase transformations at higher temperatures. Amorphous and rutile TiO_2 were found inefficient. The prepared catalyst was characterized by BET, SEM and FTIR. The surface area from BET investigated was 100 to 160 m^2 and the crystal size was about 5 to 6 nm [28].

Amit Kumar Sharma et al., 2012 synthesized ZnO nanocatalyst prepared by precipitation method. This catalyst was applied for the degradation of Methyl parathion, Parathion under UV light. The concentration of the OP pesticide in each degraded sample in various illumination time was determined using UV–Vis spectrophotometer at γmax = 395 nm for MP and at γmax =352 nm for PA. The degradation of pesticides with ZnO nanocatalyst followed the pseudo-first order kinetics. Effect of different parameteri-e Quantum Yield, Electrical Energy Per Order (Ee_o), Dosage Of Nano photocatalyst, L–H Model was studied [29].

G. Chaitanya Lakshmi, S. Ananda 2012 worked for the photo catalytic degradation of Eosin Yellow Dye with the nanocomposite ZnO/MgO**.** They synthesized the catalyst from anodic oxidation of metal. Zinc and Magnesium metal wires were used as electrodes. The catalyst was characterized by XRD, SEM, PALS, UV and IR Spectroscopy. The UV-Visible spectroscopy showed that the band gap energy of ZnO/MgO nanocomposite is 3.9 eV, according to XRD the crystallite size was17.55 nm calculated by using Williamson-Hall plot. IR spectrum revealed the presence of CO_2 and OH radicals. The PALS measurements confirmed that ZnO/MgO nanocomposite consists of more defects and vacancies than ZnO that caused improvement in photocatalytic degradation of eosin yellow (EY) dye than the pure ZnO was observed. The synthesized catalyst was treated for the decomposition of Eosin dye. The percent transmission was recorded for the solution. Chemical oxygen demand was also estimated before and after treatment using dichromate oxidation method. Factors studied were pH, Eosin Yellow concentrations, catalyst loading and light intensity [30].

Abdul Halim, Abdullah et al., 2013 worked on the degradation of Chlorophenoxyacetic Acids pesticides with the nanocomposite ZnO/γ-Fe_2O_3. They synthesized the catalyst through precipitation method, and then heated at high temperature at 450 ^oC for an hour. The nanocomposite so formed was of the size of 11 nm and area 20 m^2/g found from SEM and BET analysis respectively. The XRD pattern and Zeta potential for surface charge properties analysis were also found. Effect of pH and catalyst loading was studied; other factors i-e temperature and light intensity were kept constant [31].

Chunde Jin, Jingpeng Li et al., 2014 worked on the degradation of rhodamine pesticide at room temperature. They prepared a novel recyclable ZnO catalyst from hydrothermal method and immobilized it on bamboo through dip coating. The bamboo slices were immersed into the ZnO sol solution for 5min and then dried, the process was repeated many times until the cross linked nano walls were appeared. The so formed catalyst was characterized by FTIR, XRD and SEM. The SEM image is shown as follow;

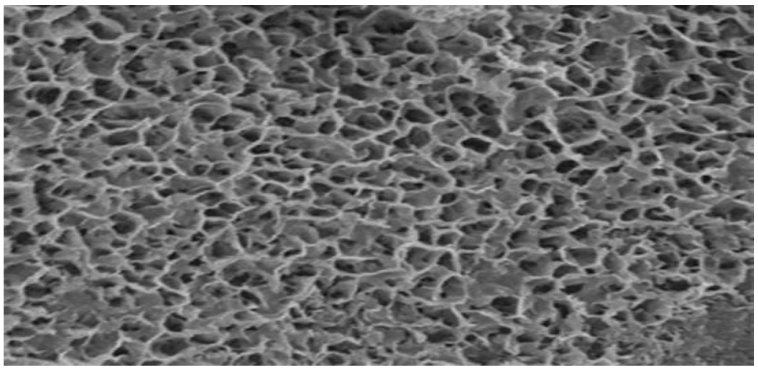

Figure 2.1 Cross-Linked ZnO nanowalls immobilized onto bamboo surface

The photo catalytic efficiency of the prepared catalyst was about 70% [32].

2.2. Titanium dioxide as photo catalyst

TiO_2 was known from 1960s experiments of A. Fujishima, and later on many researchers made it their basic ingredient to their degradation recipes.

Some of the work is discussed as follow;

Chen shifu and Liu Yunzhang, 2006 worked on the photo catalysis of TiO_2 powder for the degradation of glyphosate. Glyphosate is the organophosphorous herbicides used widely throughout the world for controlling weeds. It contaminates the ground water and soil. They prepared the TiO_2 catalyst by thermal decomposition and calcinations of the colloid obtained from the hydrolysis of titanium isopropoxide.

From their study they investigated the impact of different parameters i-e amount of catalyst, time of light illumination and initial pH value. The effect of electron acceptors, metal ions and anions was also investigated but they have very little impact[33].

J. Santhanalakshmi, R. Komalavalli, et al., 2012 synthesized nano crystalline TiO_2 for the degradation of pesticides chloropyrifos, endosulphon, imi-docloprid, Quinolphos. For catalyst synthesis they utilized a combination of hydrothermal and sol gel method. From characterization XRD showed that TiO_2 nanoparticles were anatase crystalline. SEM showed that average size of particle was 20 ± 0.05 nm. UV-Visible

spectroscopy and HPLC techniques were used to study the kinetic and reaction pathway of the photo catalytic decomposition of the compounds. From their experiment they concluded that in the absence of TiO_2 catalyst, the degradation was impossible. In their study they focused the effect of pH, and mass of catalyst. The low pH was considered to be optimum for the degradation. The pH caused variation because of its effect on the ionization states of the catalyst [34].

Marziyeh Salehi, Hassan Hashemipour, Mohammad Mirzaee 2012 investigated the kinetics and factors affecting the degradation of methylene blue with TiO_2 nanopowder. In their study they used simultaneously the photolysis and sonolysis systems for the degradation. Different parameters i-e catalyst dosage, initial concentration of dye, UV power, pH were studied. From the kinetic study they revealed the pseudo first order reaction in both photolysis and sonolysis, but for the sonolysis the rate constant was found to be higher than the photolysis. They also performed the same experiment with ZnO nano powder as catalyst, and studied their comparison. From the comparison they investigated that TiO_2 has a higher photo catalytic activity [17].

Thammasak Rojviran, Apirat Laobuthar et al., 2012 studied the photo catalytic activity of TiO_2 nano films for the decomposition of toluene. They also prepared an iron doped film as well for the comparative study of their work. The nano films were synthesized by sol gel followed by dip coating method. The structural and optical properties of these films were done by using XRD, UV vis spectrophotometry. The surface morphology and elemental analysis was done with AFM and XRF. The catalytic activity of the films was evaluated from the study of decomposition of toluene. The reaction followed the Langmuir-Hinshelwood model [35].

2.3. Photo catalytic activity modification

TiO_2 is the most promising semiconductor. It is thermally stable and photo catalytically active, but its low quantum yield and visible light utilization is the major obstacle in the practical use. To widen its application various approaches have been made i-e coupling it with some other compounds or doping metals or non-metals with it.

The photo catalytic response of TiO_2 shifts red by doping some metals or non-metals with it, or making nano composites [36]. This section is further divide into two sub section.

2.3.1. Photo catalytic studies of nano composite

As titanium dioxide nano catalyst is effective only under UV illumination, to make it active under visible light it can be coupled with other nanocatalyst. Some of the work done in this field is explained as follow;

Romana Khan, Tae-Jeong Kim., 2008 studied the synthesis and application of visible light photoactive Ni-doped TiO_2 coupled with SnO_2. They prepared Ni-doped TiO_2 by sol gel method and then SnO_2 was coupled to it through a ligand exchange reaction. Finally the catalyst was then thermally treated to form a nanocomposite. This nanocomposite was characterized by DRS spectrum, XRD and XPS. The presence of Ni and Sn on the catalyst surface was confirmed by DRS and XPS respectively. According to the XRD analysis the TiO_2 was anatase. The prepared catalyst was then applied for the degradation of toluene and its performance was compared with bare TiO_2, Ni doped $TiO_2$and TiO_2-SnO_2 [37].

Yunfei Ma, Jinlong Zhang et al., 2010 synthesized and characterized Samarium and Nitrogen co-doped TiO_2 which was thermally stable and highly active in visible light. The catalyst was prepared by using co-precipitation method and characterized by XRD, XPS, high-resolution transmission electron microscopy, FTIR and UV visible spectroscopy. From their work they revealed that doping samarium with titania inhibits the growth of crystal size and also avoid its phase change from anatase to rutile phase. The activity of catalyst was then studied by the degradation of salicylic acid under visible light irradiation [38].

Yanhui Zhang, Zi-Rong Tang et al., 2011 studied the catalytic activity modification of Titania by coupling it with Ag-AgBr. They synthesized the nanocomposite by modified deposition precipitation method. The so formed catalyst was durable, thermally stable and highly photo catalytic. The morphology, structure and optical properties of the catalyst were determined from TEM, XRD and UV-Vis diffuse

reflectance spectra. The FTIR analysis showed the chemical bonding of O-Ti-O, and the XPS was used to investigate the surface adsorption of Ag/Ag-Br over the catalyst. The activity of the catalyst was evaluated from the gas phase decomposition of volatile compounds in air, aromatic benzene and non-aromatic acetone [39].

Feng Wang, Kan Zhang, 2011 synthesized a nanocatalyst graphene oxide–TiO_2 for the photo decomposition of pesticide Rhodamine B. Graphene oxide–TiO_2 nanocomposite were synthesized with different weight ratios of GO and P25 i-e (1:100, 1:40, 1:20, 1:10 and 1:3) by a hydrothermal method, then heated at 400 °C for 2 h under Argon atmosphere. During this hydrothermal reaction, the reduction of GO to graphene can be completed by depositing TiO_2 onto the graphene sheets. The catalyst was then used for the degradation of the pesticides. The concentration declination was investigated by UV–visible spectroscopy. The concentration of Rh.B in the solution was determined as a function of irradiation time from the absorbance region at a UV wavelength line of 555 nm [40].

Jurate Virkutyte, Veeriah Jegatheesan, Rajender S. Varma, 2012 studied the enhanced properties of hybrid inorganic/organic nanocomposite. From their work they investigated the photo catalytic activity of hybrid TiO_2/microcrystalline cellulose for the treatment of organic contaminants in water. The catalyst was synthesized from sol-gel method. The catalyst was characterized by XRD, SEM, TGA, HR-TEM, BET and XPS. The prepared catalyst was then applied for the degradation of methylene blue [41].

2.3.2. Photo catalytic studies of doping TiO_2

The doping is further divided into two types metal doping and non-metal doping.

- ***Metal Doping***

Metal doping enhances the photo catalytic efficiency of titanium dioxide.

Scot T. Martin, Colin L. Morrison et al., 1994 doped Vanadium on titania to study the photochemical decomposition of chlorinated hydrocarbons i-e 4-chlorophenol. The catalyst was prepared by standard co-precipitation method and then followed by

calcination. The prepared catalyst was characterized by TEM, X-ray analyzer and FTIR. The 4-chlorophenol was decomposed to benzoquinone, and hydroquinone [42].

Jina Choi, Hyunwoong Park et al., 2010 used about thirteen different metal ions i-e silver, rubidium, nickel, cobalt, copper, vanadium, ruthenium, iron, osmium, yttrium, lanthanum, platinum and chromium for doping with titania. The catalyst was synthesized by sol gel method and was then characterized by XRD, SEM and XPS. The so formed catalysts were applied for the decomposition of phenol and photo bleaching of methylene blue [43].

Venkata Bharat Ram Boppana, Raul F. Lobe, 2011 doped tin Sn(II) on titania to increase the photocatalytic activity of titania. The properties of catalyst were studied by XRD, UV vis diffuse reflectance spectroscopy, DRS, XPS, IR spectroscopy, photo luminous Raman spectroscopy. The prepared catalyst was used for the decomposition of rhodamine B dye [44].

Kanakkanmavudi B. Jaimy, Swapan Kumar Ghosh et al., 2011 prepared Cr(III) doped titanium dioxide by sol gel method. They revealed the red shift in photo response of titania by doping with chromium metal. The as prepared catalysts was characterized for structural and optical properties and then applied for the decomposition of methylene blue dye [45].

T. Siva Rao,Teshome Abdo Segne et al., 2012 worked on the photo catalytic activity of titania doped with magnesium ion for the decomposition of Dichlorvos pesticide in sunlight. The catalyst was synthesized by sol gel method followed by calcination and aging for about 48 hours. The morphology, crystalline structure, size and optical properties were determined from SEM, XRD, XPS, BET and diffuse reflectance spectroscopy. Photo catalytic efficiency of the as prepared catalyst was elucidated from the decomposition of aqueous dichlorvos pesticide. Parameters studied were dopant concentration, pH of solution, dosage of catalysts, and initial pesticide concentration [46].

Titania doped with metals or metallic cations have a very high catalytic activity but metal doping has also some demerits. The metal doped TiO_2 is thermally instable, the

metal blocks the active sites on the surface of titania and the ion implantation is very expensive [47].

- ***Non-metal doping***

Jirapat Ananpattarachai, Puangrat Kajitvichyanukul, Supapan Seraphin, 2009 worked on synthesis, characterization and kinetic study of various interstitial N-doped $TiO_2$and reported comparison of different nitrogen sources i-e diethanolamine, triethylamine and urea. The prepared the catalyst by sol-gel method. The catalyst was characterized by XRD, XPS, TEM and UV visible spectroscopy and was used for the degradation of 2-chlorophenol. From this work they investigated that among the above nitrogen sources diethanolamine found to have the higher visible light absorption ability of interstitial N-doped TiO_2, the catalyst so formed has smallest energy band gap and smaller anatase crystal size and thus results in the highest efficiency [47].

Police Anil Kumar Reddy, Pulagurla Venkata Laxma Reddy et al., 2010 studied the photo catalytic activity of C, N and S doped TiO_2 for the degradation of pesticide isoproturon. For the catalyst synthesis they used a hydrolysis process. The prepared catalyst was characterized by XRD, SEM, XPS, BET, FTIR and diffuse reflectance spectra. For the degradation of the pesticide, aqueous isoproturon solution of 50 ml was poured in an open glass vessel with certain amount of the catalyst. The solution was then illuminated with sun light. Distilled water was added periodically to avoid concentration changes due to evaporation loss [48].

Xi-Kui Wang, Chen Wang et al., 2011 synthesized N-TiO_2 through a novel sonochemical process. The catalyst so prepared was in anatase form even at low temperature. The catalyst was in anatase form, and its preparation was affected by the reaction time and temperature. The catalyst was then characterized by XRD, XPS, TEM and UV visible diffusion spectrum. The XRD showed that at lower sonication temperature up to 50 ^oC, the catalyst is in crystalline form, increasing the temperature up to 80 ^oC made it anatase. The sonication time has also impact on the catalyst morphology. The average crystalline size found from the XPS analysis was about 10.8 nm. The TEM revealed the weight percentage of nitrogen i-e 3.66 to 4.25.The UV

visible diffusion spectrum confirmed that nitrogen doping shifts the absorption edge to larger wavelength. In this work the photo catalytic efficiency of the prepared catalyst was investigated from the decomposition of azo dye direct sky blue [49].

Halide Diker, Canan Varlikliet al., 2011 worked on the characterizations and photo catalytic activity of N-doped TiO_2 depending on synthetic conditions and structural differences of amine sources prepared N-doped TiO_2 nanoparticles by hydrothermal growth method. The catalyst was then characterized by XRD, SEM, UV visible absorption spectra, XPS, FTIR and BET analysis techniques. The Nitrogen composition in the catalyst was found to be depended on the synthesis techniques, the conditions and the sources of nitrogen. The prepared catalyst was used for the photo catalytic degradation of methylene blue.

Parameters studied were acidity of the amine sources, irradiation time and different preparation techniques [50].

P.V.R.K. Ramacharyulu, J. Praveen Kumar et al., 2014 studied the photocatalytic activity of Sulphur doped titania for the decomposition of sulphur mustard ($C_4H_8SCl_2$, 2, 2'-dichloro diethyl sulfide) in sunlight. Sulphur mustard is a toxic compound causing death of cells, harmful for DNA. The catalyst was prepared by sol gel method followed by hydrothermal treatment. Thiourea was used as a source of sulphur for doping. The so formed catalyst was then characterized by XRD, TEM, XPS, BET and FTIR. The following is the XPS image;

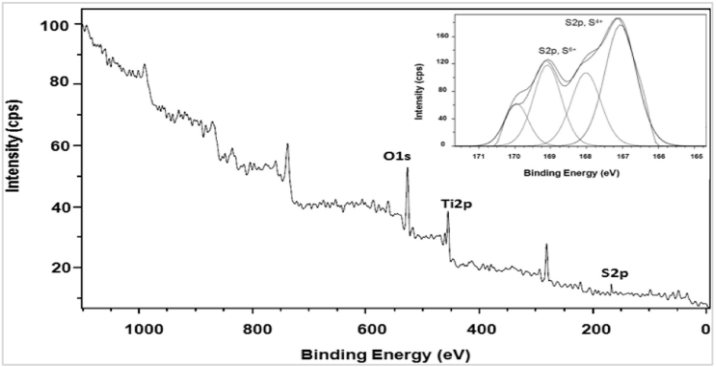

Figure 2.2 XPS image of Sulphur doped TiO_2

The degradation was evaluated by using gas chromatography mass spectrometry. The catalytic activity of doped titania was compared with that of undoped. The sulphur doping was found to enhance the photo catalytic efficiency [51].

2.4. Photo catalytic degradation of OP pesticides

Organophosphorous (OP) pesticides contaminate the soil and water bodies and stay for long thus prove fatal for the human environment. A lot of research has been done for the degradation of these pesticides. This section explains the worked carried out for the degradation of acephate and omethoate pesticides.

2.4.1. Acephate degradation

Acephate also called orthene, stays in the environment for about 50 days and it is soluble in water. It undergoes hydrolysis at very slow rate [52].

Acephate degrades to methamidophos which is another organophosphorous pesticide. The methamidophos inhibits acetyl cholinesterase through phosphorylation. The acephate can also be transform into S-methyl acetyl phosphoramidothiolate which is not an acetyl cholinesterase inhibitor.

Glory Rose Mangat Echavia, Fumiko Matzusawa, Nobuaki Negishi 2009 studied the degradation of two pesticides acephate, dimethoate and herbicide i-e glyphosate. The investigated the photo catalytic activity of TiO_2 immobilized on silica gel. For their study they synthesized anatase TiO_2 from simple sol gel method and then immobilized on silica.

The advantage of immobilization they discovered was that no toxic intermediates were detected during the degradation and the pesticides were completely mineralized to carbon dioxide, inorganic ions and water. The proposed the following mechanism for the acephate mineralization;

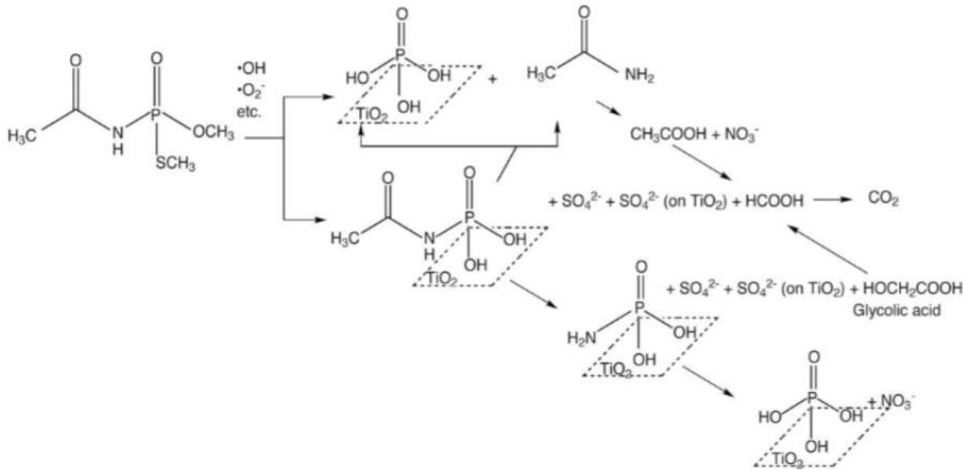

Figure 2.3 Proposed mechanism for the acephate decomposition

The decomposition of acephate and dimethoate was efficiently photo catalytic, pseudo first order following Langmuir–Hinshelwood kinetics, while the degradation of glyphosate was also done by adsorption [53].

Wang Shu-Wei, He Chi et al., 2012 worked on the degradation of acephate pesticide. They elucidated the activity modification of titiania by doping it with $ZnFe_2O_4$ and compared its performance with another catalyst $ZnFe_2O_4$. The nanocatalysts were synthesized by sol-gel and co-precipitation methods respectively. The catalyst morphology and optical properties were studied by characterizing it with XRD, TEM and UV-vis DRS. The initial pH value, catalyst dosage and concentration of H_2O_2 were the affecting parameters [54].

Xinlei Zhang, Jaun Zhou et al., **2014** studied the photo catalytic behavior of N-doped TiO_2 nanotube arrays by degrading acephate pesticide. The methodology they adopted for the catalyst synthesis was anodic oxidation of Ti electrode with Platinum electrode, and finally calcinations of the thin film obtained in N_2 atmosphere. The catalyst was characterized by SEM, XRD, and XPS. Their work showed that Nitrogen doping does not change the structure of TiO_2. According to SEM the particle diameter was 40 nm, wall thickness was 12 nm. Raising the temperature for annealing decreases

the nanotube diameter and increases the wall thickness, along with causing the opening coarser. The cross section of SEM showed the walls are smooth, open from front but closed from bottom and is hemispherical dome structure. At some points the wall is ruptured. The XRD showed that before annealing the TiO_2 prepared by anodic oxidation was amorphous, after annealing in N_2 atmosphere at 400 ^oC the TiO_2 transformed to anatase form. The Nitrogen replaces Oxygen in TiO_2 causing increase in the compressive strain due to the difference in the binding properties; it was shown by the broadening of XRD peaks and reduction of peak area. Annealing up to 600 ^oC changed the anatase to a rutile one. They also suggested that the electron binding energy and electron density of Nitrogen in N-Ti-O is higher than N-Ti-N due to high electro negativity. The Ti 2p peaks were symmetrically distributed around 458.6 eV and 464.4 eV. The catalyst was used for the degradation of acephate which is low degrading pesticide. UV vis spectrophotometer was used to record the absorbance of the decreasing concentration of pesticide and catalyst solution [55].

2.4.2. Omethoate degradation

Omethoate is the most widely used pesticides. They are neurotoxic as they inhibit acetyl cholinesterase. They are serious hazard to the human environment. Their half-life is more than 68 days. The following work has been done for its degradation;

Zhao Xiu-Feng, Meng Xian-Fenget al., 2004 prepared lead doped titania films, and their catalytic activity was investigated from the degradation of omethoate pesticide and decoloration of methyl orange. The catalyst films were synthesized on the surface of active carbon through a sol-gel dip-coating method. The thin films were characterized by UV-vis spectrophotometry, TEM and XRD [56].

Tao Yugui, Wang Yaoming et al., 2008 worked on the process optimization of omethoate degradation and explained the kinetics of the reaction. For their study they focused on the biodegradation of pesticides by microorganisms, as it was the most effective method used for environmental remediation. They studied its biodegradation by Aspergillus niger. For the optimization of process conditions they used the response surface method. From this work the effect of concentration of glucose, initial pH value

and the culture temperature on omethoate degradation was revealed. The reaction was of first order kinetics and catalyzed by an enzyme released by the microorganism used. The intermediate suggested for this degradation were 2-mercapto-N-methylacetamide and dimethyl hydrogen phosphate. The optimum conditions investigated for the decomposition were 1.9% glucose concentration, initial pH 6.21, and a culture temperature of 32.64 ºC [57].

Zhao Di-Shun, Wang Jia Lei et al., 2009 investigated the photo catalytic degradation of omethoate pesticide with a NaY zeolite supported TiO_2 nanocomposite. The catalyst was synthesized by sol gel method and calcined at different temperatures. The prepared catalyst was characterized by XRD, SEM, BET and FTIR. Hydrogen peroxide was used as an oxidant to facilitate the formation of hydroxyl ions that initiate the degradation reaction. The parameters studied for this degradation were the calcination temperature, omethoate initial concentration, amount of catalyst adsorbed over the zeolite surface, amount of catalyst used for degradation, and hydrogen per oxide concentration. The kinetics of the reaction were studied and showed that this degradation was of first order [58].

Chapter 3: Experimental work

This chapter explains all the practical work performed for the synthesis of TiO_2nanoparticles and its doping with Nitrogen. This chapter also discusses the details of the off- line-techniques used for the characterization of as prepared nanocatalyst.

3.1. Synthesis of TiO_2 nanoparticles

The practical work of the research started with the preparation of TiO_2 nanoparticles. The nano sized TiO_2 were prepared by simple sol gel method.

3.1.1. Materials

Titanium tetraisopropoxide (Sigma Aldrich), 2-propanol (Sigma Aldrich), distilled water; nitric acid and urea were used for the nanocatalyst.

3.1.2. Procedure for the synthesis of TiO_2 nanoparticles

The TiO_2 nanoparticles were synthesized by using the sol gel method. All the experiments were carried at room temperature. All the experiments were performed by using the following steps;

3.1.2.1. Preparing the colloidal solution

The first step was the formation of a milky colloid, which turns to a transparent solution after sometime, this colloid was prepared by taking 900 ml distilled water in a conical flask and stirring it on a magnetic stirrer. While being stirred a few drops of nitric acid was added to maintain the pH of the water up to 2. Then 5 ml titanium tetra isopropoxide dissolved in 95 ml 2-propanol was added drop wise from a dropping funnel at the rate of 1 ml per minute.

This solution was kept on stirring for about 24 hours at room temperature in air. After 24 hours an opaque/cloudy colloidal solution was obtained.

Figure 3.1 colloidal solution formations

The colloid was then dried in a rotary evaporator at 60 ^{o}C and 120 rmp. The drying took about 12 hours. The dried powder was put in vacuum dryer for further removal of moisture.

Figure 3.2 Drying in rotary evaporator

The dried powder was taken out and characterized with SEM and XRD to analyze the particle size distribution and morphology.

After size confirmation the nano powder were doped with different percent of Nitrogen. Urea was selected as the source of Nitrogen dopant. The procedure of doping is explained below.

3.1.3. Procedure for nitrogen doping

The nanoparticles of TiO_2 obtained from the above experiments were then nitrified with urea. The nitrification was done by the following procedure.
Different amount of urea was mixed with 1 gm. of TiO_2 and ground well for 30 minutes.

Figure 3.3 Mixing and grinding Urea and nano powder of titania

The mixture was then calcined at 400 ^{o}C for 1 hour. After one hour the N-doped TiO_2 were obtained and the powder was ground again and its particle size distribution, morphology, chemical composition and surface area was found from different characterization techniques.

Table 3.1 Indices of samples and experimental details:

Sample index	Sample composition	Calcination Temperature	TiO_2:Urea (mass ratio)
bulk TiO_2	bulk TiO_2	-	-
SN-0	Pure nano sized TiO_2	400 ^oC	1:0
SN-0.1	nano sized TiO_2 + Urea	400 ^oC	1:0.1
SN-0.5	nano sized TiO_2 + Urea	400 ^oC	1:0.5
SN-1	nano sized TiO_2 + Urea	400 ^oC	1:1
SN-2	nano sized TiO_2 + Urea	400 ^oC	1:2
SN-3	nano sized TiO_2 + Urea	400 ^oC	1:3

3.2. Characterization of the catalysts

Particle size distribution, elemental analysis, morphology, crystalline phase of the prepared catalyst, surface area was found by using different characterization techniques. The above properties were distinguished under two main types; the structural and optical properties.

3.2.2. Structural properties

The properties under this heading include the morphology, crystalline phase, topography and elemental analysis. The following techniques are used for studying such properties;

3.2.2.1. Scanning electron microscope (SEM)

Morphology, topography and crystallography were studied from SEM characterization. Morphology means the size, appearance and arrangement of the particles. Topography shows the surface characteristics of the sample and crystallography is related with the atomic arrangement of the material.

SEM images were taken by JEOL JSM-6460. The instrument of SEM uses a highly energetic beam of electrons instead of light for optical microscopy. The following is the schematic diagram of SEM.

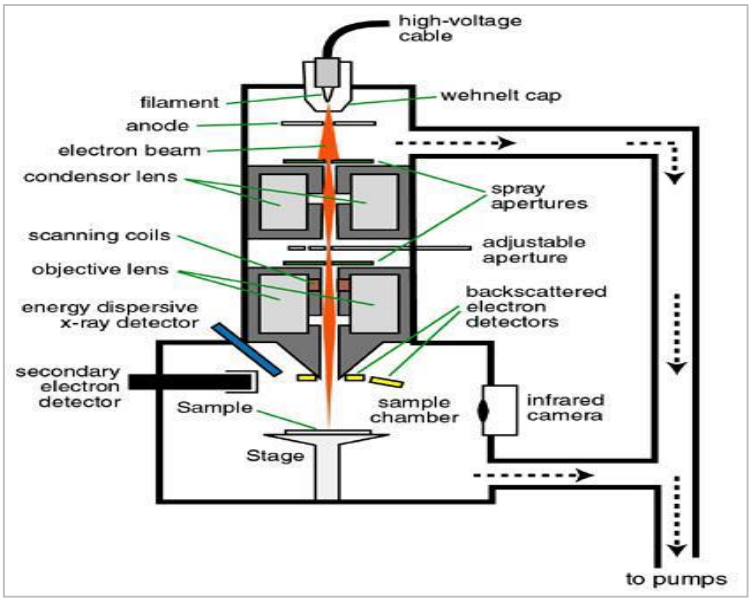

Figure3.4 Schematic diagram of scanning electron microscope (SEM)

The main parts of this instrument are electron optical column, vacuum system and signal detection and a display system as shown in the figure below. The optical column contains magnetic lens, electron source and apertures. Vacuum is created by a vacuum pump. Condenser lens in the instrument confines the electron beam from the electron gun. The second condenser lens which is controlled by current knob, make the electron beam coherent. The objective lens focuses this beam on the sample material. As the electron beam interacts with the material, signals are produced which are detected by the detector.

3.2.2.2. Energy dispersive spectroscopy

EDS is the analytical technique that is used for finding the elemental composition of a given sample. The EDS is hyphenated with SEM from there it collects the data and the elemental composition of the given sample is then found from the data. The different elements are distinguished from their characteristic x-rays emitted when highly energetic beam of electrons hits these samples. The x-rays emitted falls on the detector and a spectrum is then drawn that shows different peaks specific to the elements present. So by using the energy dispersive X- ray spectroscopy technique the elemental

composition of the sample can be predicted accurately. Schematic diagram of different parts of EDX is shown in the Figure 3.5.

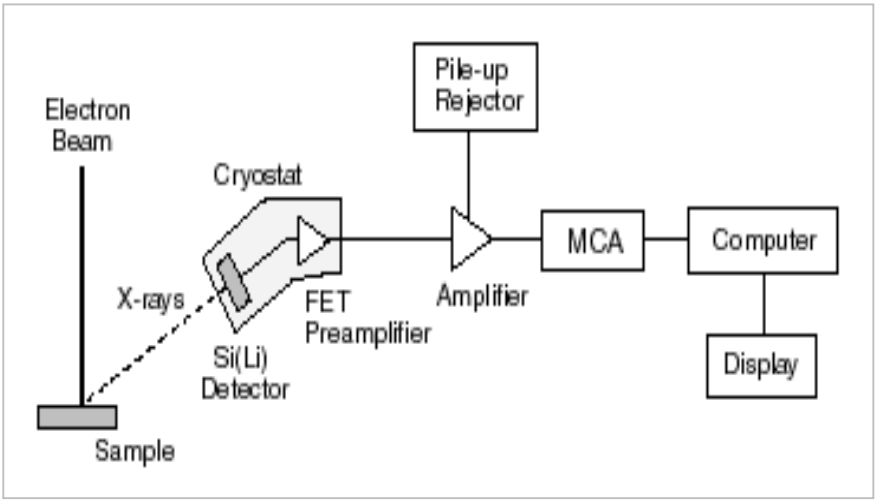

Figure 3.5 Schematic diagram of EDX

3.2.2.2. X- ray diffraction

XRD is among the unswerving techniques used for elucidating the morphology and phases in different component mixtures. As the intensity of the diffraction pattern of a phase in a mixture depends on concentration so it makes the quantification possible.

XRD analysis of TiO_2 nanoparticles and nitrogen doped TiO_2 was made by JEOL JDX-II, X-ray diffractometer. XRD is used to find atomic size, crystal structure, phases, orientation and defects in crystal structure, strain and stress of the crystalline materials. There are two modes of operation for the XRD. The angle is set wide in one mode while in the second mode a small angle is set to study the diffraction pattern. But the key setup for the XRD remains the same. Every material has its characteristic XRD pattern when subjected to the emitted X-rays.

Initially the X-rays are generated, then these radiations interact with the sample material and the data is obtained and interpreted as peaks. The whole process is as shown in the Figure 3.6. For the x-rays production the electrons are excited and accelerated inside the tube to strike the target materials with high voltage. The target materials are usually transition metals i-e copper, chromium etc. The inner shell transition of electrons in the atoms of these transition metals produces the X-rays

emission. The X-rays spectrum is composed of different types of x-rays i-e Kα, Kβ and Kγ depending on the electron excitation from the different energy levels.

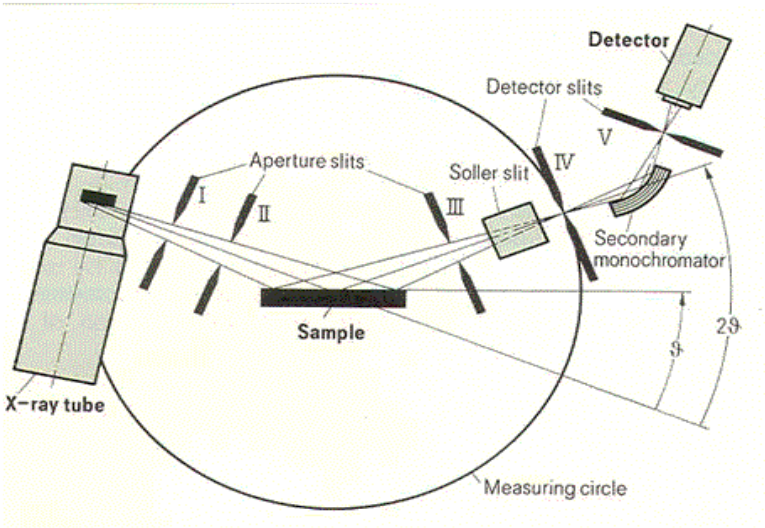

Figure3.6 X- ray diffraction scheme

These X-rays are filtered by a monochromater as every target material has a unique and specific wavelength x-rays. After filtering out through the monochromater, the x- rays are then bombarded on the material to be analyzed. After targeting the material, the X-rays reflect back, are being detected through the detector and on converted into signals; interpretation is done by a computer program. XRD data can also provide the information of the particle size of the crystallite by applying the Scherer's formula ($D= K\lambda / B\cos\theta$).

3.2.2.4. Surface area measurement by BET analysis

The surface area of the prepared catalysts was found from BET analysis by using model NOVA 2200e Quanta Chrome, USA. In this equipment liquid nitrogen is used for adsorption. Degassing of all samples is carried out at 300^{o}C for several hours and then adsorption of the liquid nitrogen is done. Measured quantity of the catalyst sample is taken in a tube. When the degassing process is done the sample is put in a sample holder and the helium gas is passed to create inert atmosphere and then nitrogen is passed for adsorption.

3.2.3. Optical properties

The optical properties for the catalyst samples are found by using the following techniques;

3.2.3.1. Fourier transforms infrared spectroscopy

FTIR spectroscopy gives information about the functional groups present in the provided chemical compound. This is a non-destructive analytical technique that can give the qualitative analysis as well as quantitative analysis. The sample is subjected to infrared radiations. These radiations interact with the sample and produce bending or stretching vibrations at different frequencies that match with the frequency of the bonds present in the compound.

The molecules in the compounds absorb the IR radiations and are excited from ground energy state to higher energy state gaining higher vibrational amplitude. This spectroscopy is thus also a vibrational spectroscopy. The vibrations that are associated with the vibrations of each bond or functional group are fundamental vibrations. Fundamental vibrations are classified as stretching and bending vibrations. The stretching vibrations have higher frequency and can change the bond length and the bending vibrations have lower frequency and can change in bond angle.

FTIR spectroscopy can be used to identify the organic and inorganic compounds. The bonding in metal-oxygen and hydroxyl in my samples was obtained through FTIR spectroscopy. For powdered samples, the sample was mixed properly with the KBr making a transparent KBr pellet by pressing it through a die. A range of 400 - 4000 cm^{-1} was selected to take the spectra on FTIR spectrometer (Tensor-37, Bruker Corporation). The results obtained in graphical form between percent transmittance or absorbance on x-axis and wave number on y- axis resulting peaks related to different functional groups.

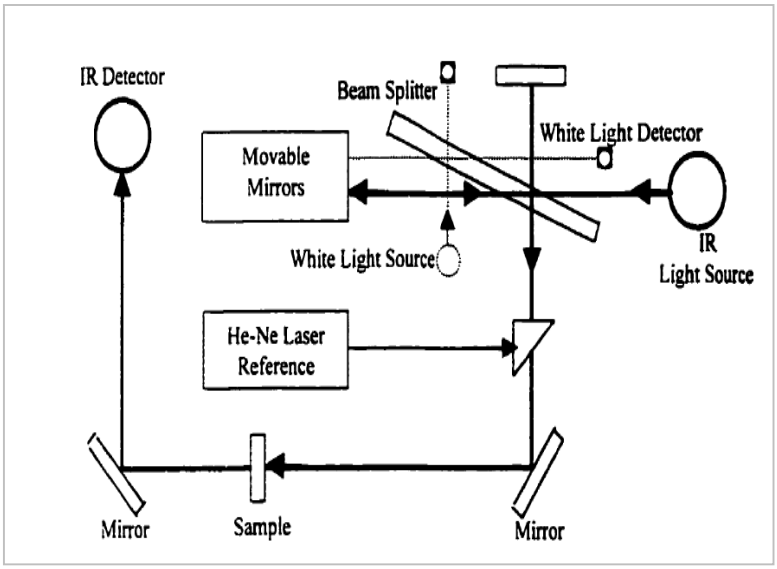

Figure 3.7 Schematic diagram of FTIR

3.2.3.2 UV- visible spectroscopy

Ultraviolet radiations are of shorter wavelength than visible radiations ranging from 200 nm to 380 nm. UV-visible ranges from 200 nm- 800 nm.

The excitation of electrons is done when a molecules absorbs the UV radiations. In double beam spectrophotometer the light splits after passing through different slits and entered into two cells, in which the sample to be analyzed and a reference sample is present.

The instrument compares the intensities of the beams and scans the required range of wavelengths. When a specific wavelength light is absorbed by the sample, variation in the intensities of reference beam and sample beam will occur.

UV- visible spectrophotometer shows the spectrum of the sample and records the wavelengths and plot these wavelength and absorption in an XY graph. The band gap (E_g) can then be computed from a Tauc plot by extrapolating the linear portion of $(\alpha h\nu)^{1/2}$ verses photon energy ($h\nu$) by using the given relation.

$$\alpha h\nu = A(h\nu - E_g)^{1/2}$$

UV-visible spectroscopy is a useful technique for all kind of quantitative analysis. We use the Bouguer-Lambert-Beer law for the calculation of light absorption which is valid for samples in solution form only. While for the case of solid samples this law is not valid due to the decrease in light intensity. The decrease is caused by interruption of absorbed light by reflection, refraction, and diffraction.

Chapter 4: Results and Discussion

This chapter explains the characterization and structural changes of the as prepared TiO_2 nanoparticles and the Nitrogen doped TiO_2 catalysts. After this the chapter includes the degradation studies of acephate and omethoate pesticides with the synthesized catalyst.

4.1. Results of the structural and optical properties of the catalysts

The structural properties of as prepared catalyst were studied from the characterization of the catalyst. Some of the results are explained as under;

4.1.1. Scanning Electron Microscopy results

SEM images for the Bulk TiO_2 and all the synthesized Nitrogen doped nano TiO_2 were taken and compared. The image for the bulk titania showed that the particles are bigger in size, having an average size above 100 nm. The particles are spherical as shown by Fig. No. 4.1

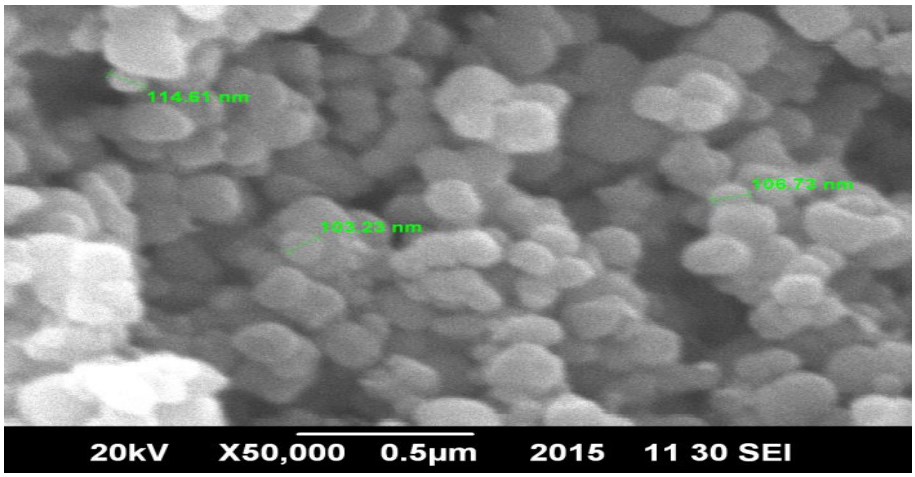

Figure 4.1 SEM image with particle size for bulk TiO_2

The as prepared nanocatalyst images show that the average particle size below 50 nm. The morphology of the particles is purely spherical. Fig. No. 4.2, 4.3, 4.4, 4.5 and 4.6 showed the Nitrogen doped titania with different percentages of Nitrogen symbolized as SN-1, SN-2, SN-3, SN-0.5 and SN-0.1.

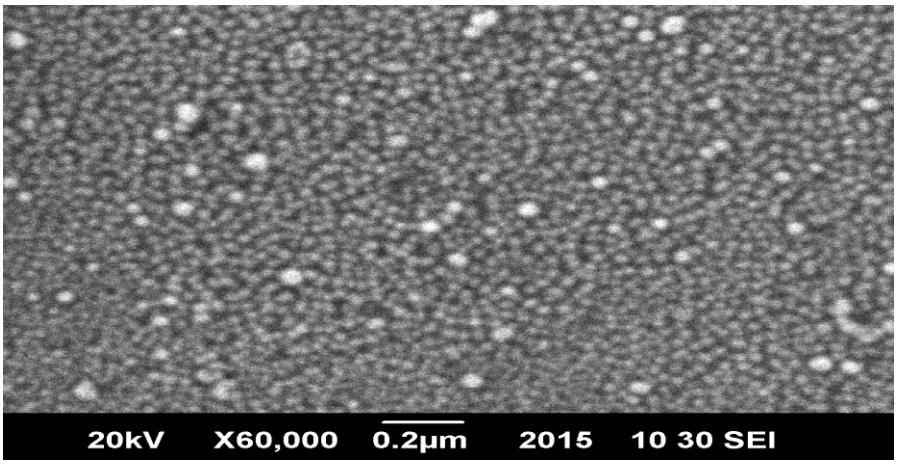

Figure 4.2 SEM image with particle size for N-doped TiO_2 (SN-1)

The ratio of urea reacted with the as prepared nanoparticles of TiO_2 in SN-1 nano catalyst is 1:1. The image shows the spherical nano particles of average size of 30 nm.

Figure No. 4.3 shows the SEM image of SN-2 nanocatalyst having nitrogen source twice as titania. The image shows average particle size of 17 nm, having spherical morphology.

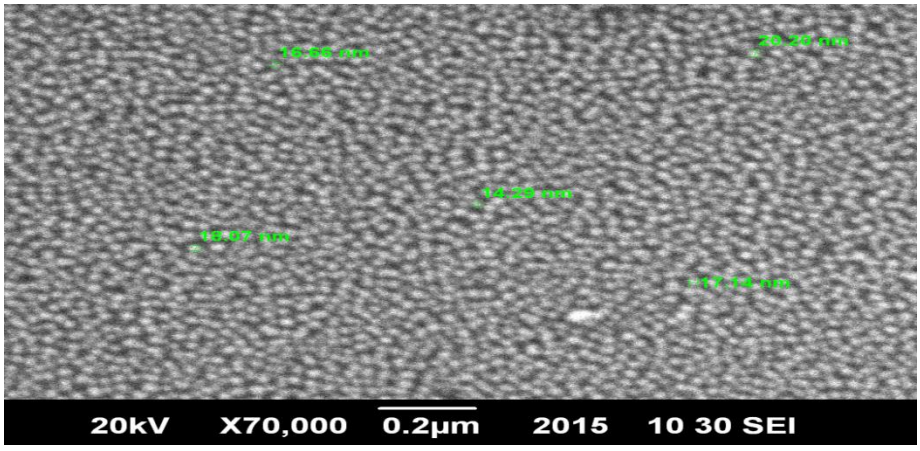

Figure 4.3 SEM image with particle size for N-doped TiO_2 (SN-2)

Then figure 4.4, 4.5 and 4.6 show the images of N-doped TiO_2 entitled as SN-3, SN-0.5 and SN-0.1. The average particle size is approximately below 35 nm.

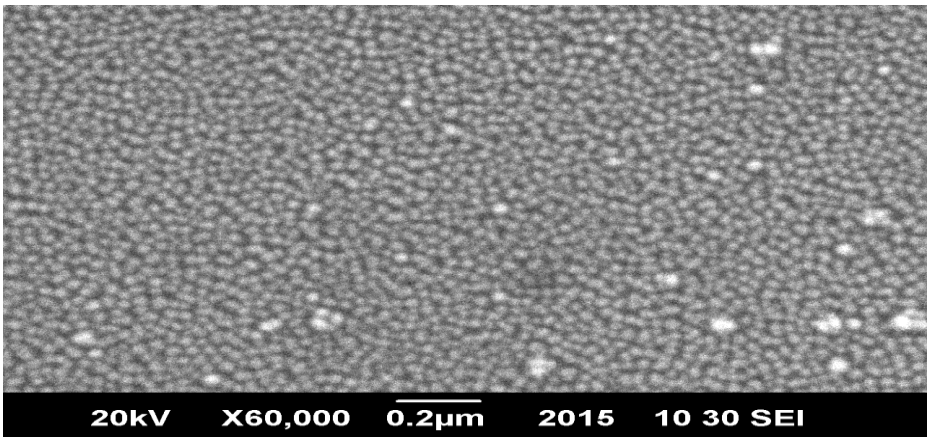

Figure 4.4 SEM image with particle size for N-doped TiO_2 (SN-3)

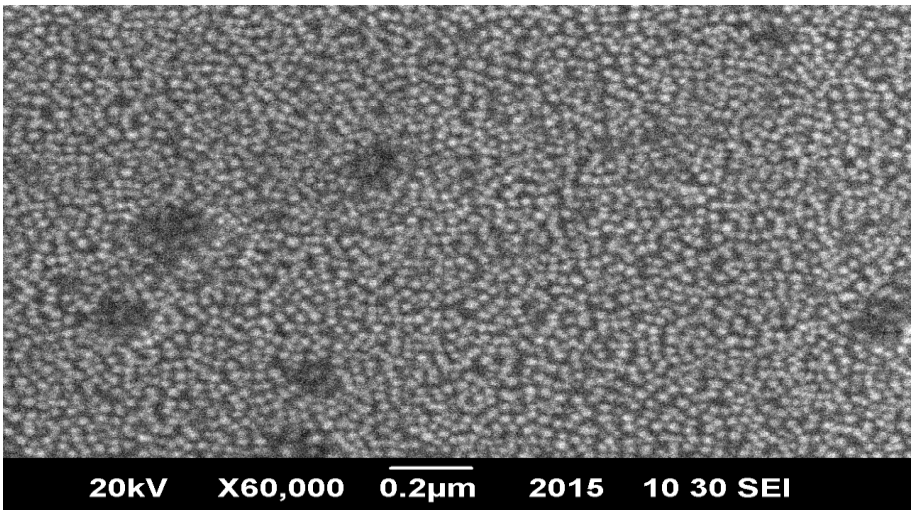

Figure 4.5 SEM image with particle size for N-doped TiO_2 (SN-0.5)

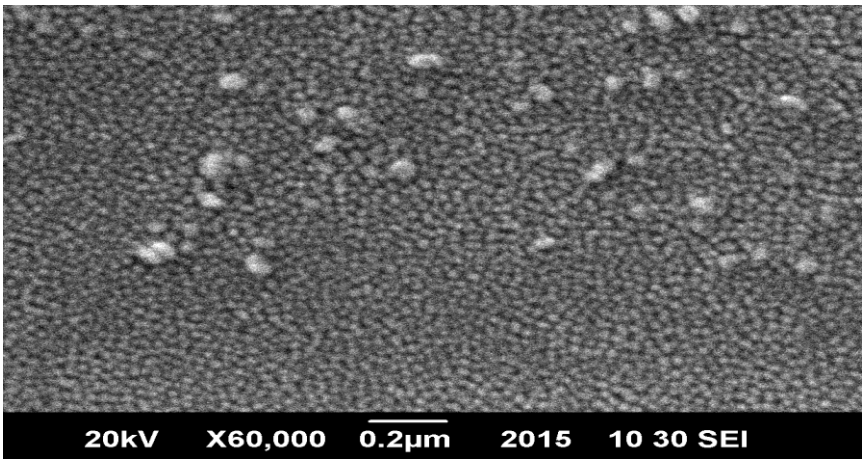

Figure 4.6 SEM image with particle size for N-doped TiO_2 (SN-0.1)

The last image (Figure No.4.7) shows the undoped nanocatalyst. The average size is about 17 nm.

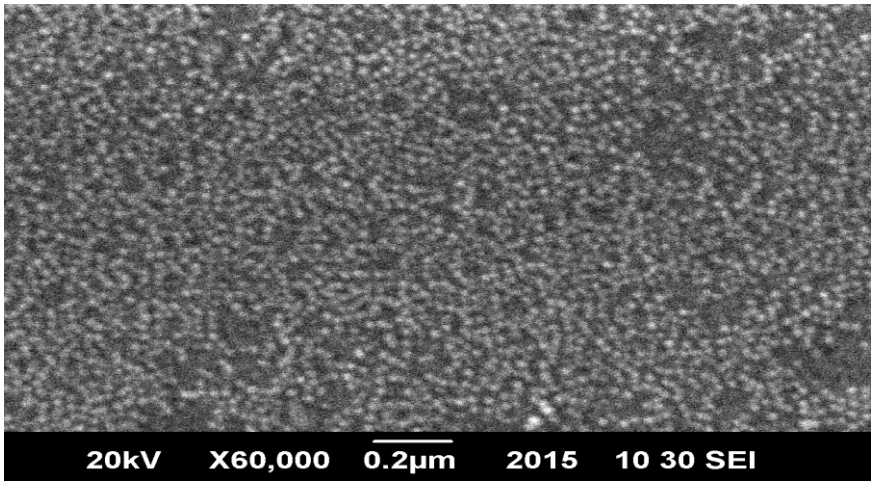

Figure 4.7 SEM image with particle size for undoped TiO_2 (SN-0)

4.1.2. Energy dispersive X-ray spectroscopy (EDX)

The mass percentages of all the elements present were evaluated from the energy dispersive X-ray spectroscopic study of the solid powder. The signals for the element present reflect the composition of each catalyst. The EDS clearly shows the signals for

only three or two compounds i-e Titanium, Oxygen and Nitrogen. The EDS for all the synthesized nano catalysts and the Bulk Titania is given in the following figures;

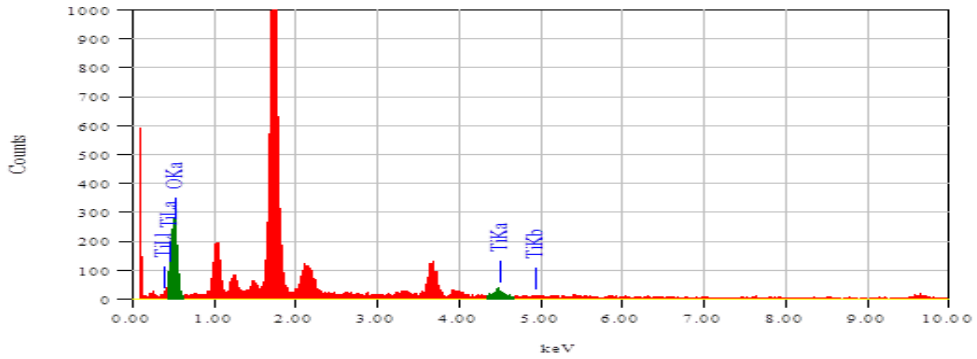

Figure 4.8 EDS for the bulk TiO_2

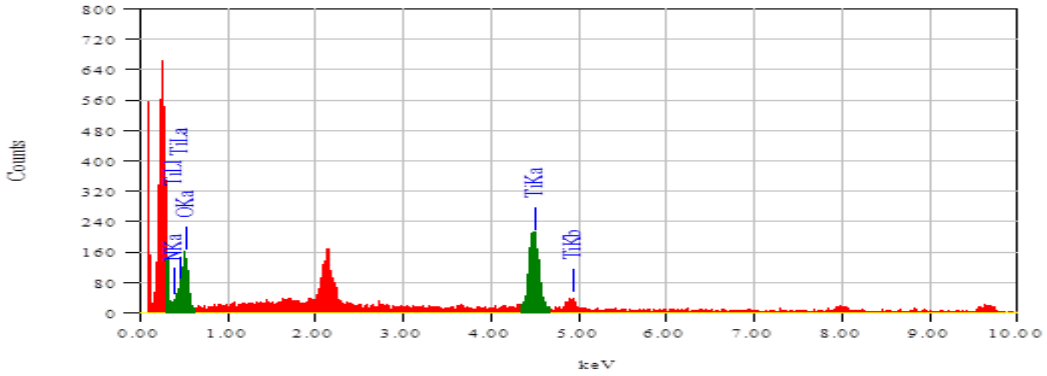

Figure 4.9 EDS for the nano synthesized catalyst SN-1

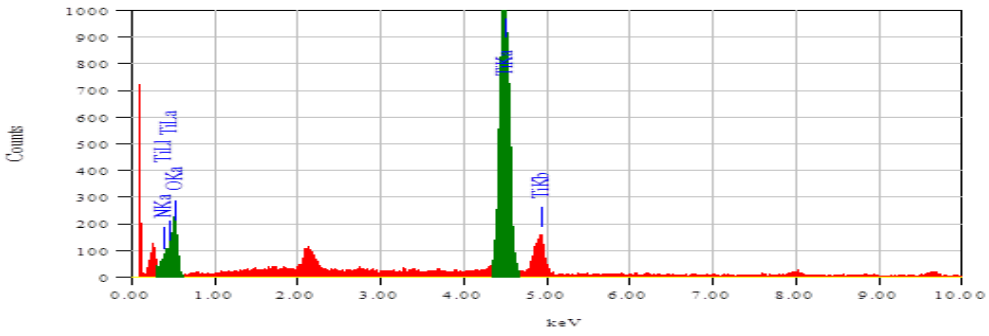

Figure 4.10 EDS for the nano synthesized catalyst SN-2

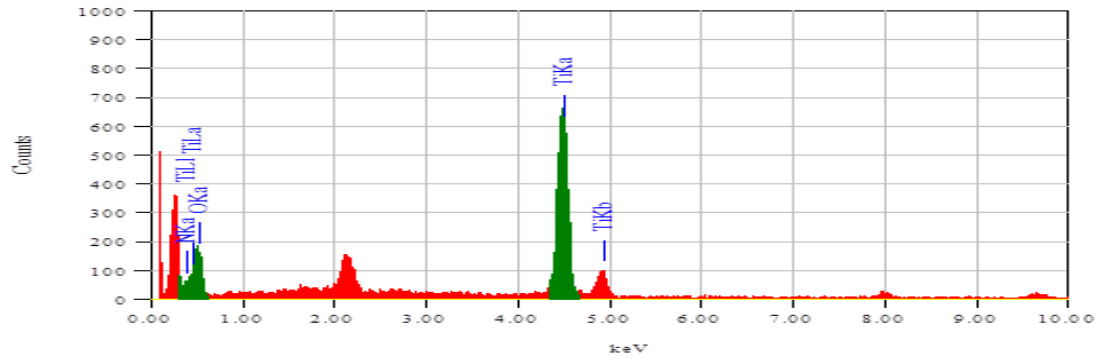

Figure 4.11 EDS for the nano synthesized catalyst SN-3

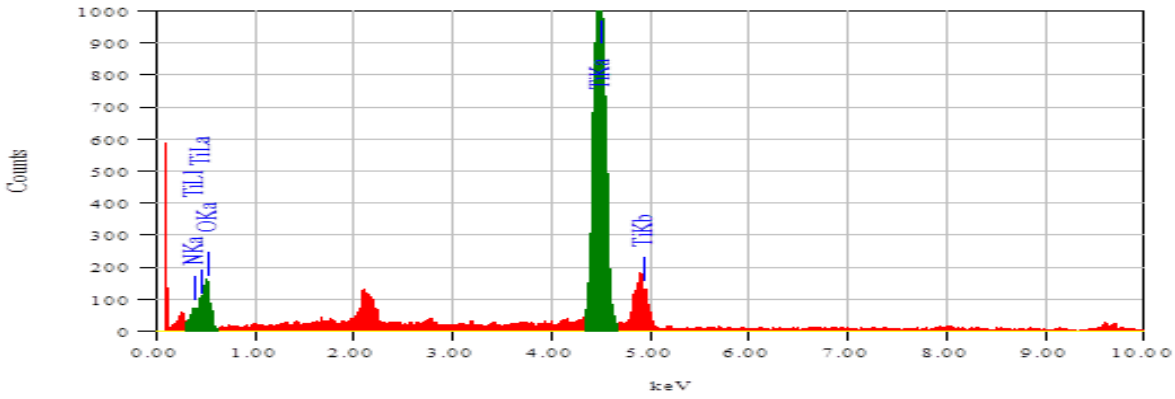

Figure 4.12 EDS for the nano synthesized catalyst SN-0.5

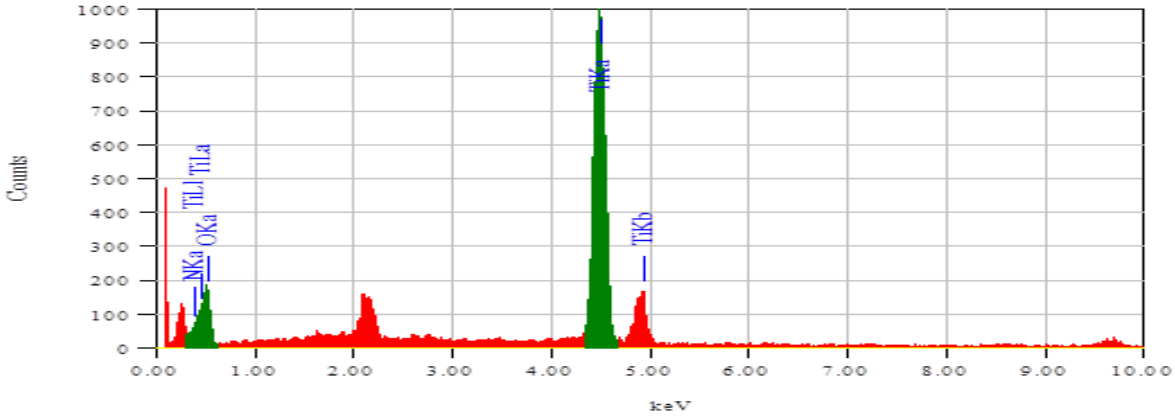

Figure 4.13 EDS for the nano synthesized catalyst SN-0.1

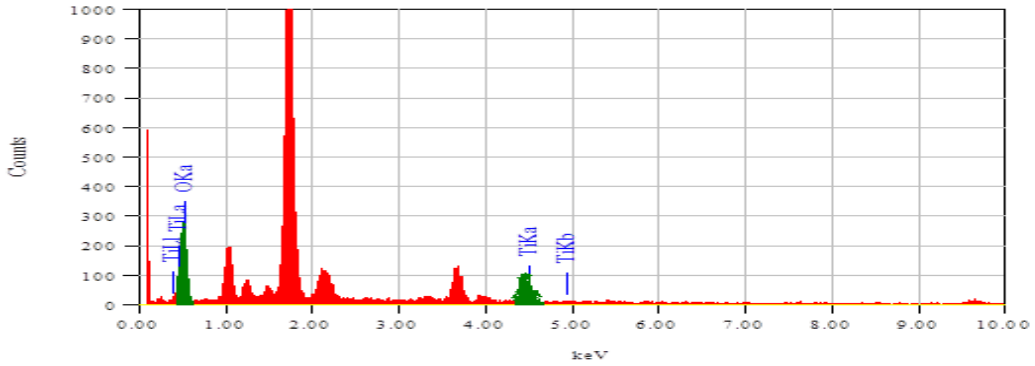

Figure 4.14 EDS for the nano synthesized catalyst SN-0

Table 4.1 Percentage composition of all elements in the synthesized nanocatalyst:

Sample Code	Atomic % of N	Atomic % of Ti	Atomic % of O
bulk TiO_2	--	28.54	71.46
SN-0	--	28.46	71.54
SN-0.1	1.06	32.98	65.96
SN-0.5	1.21	32.86	65.93
SN-1	2.42	32.53	65.05
SN-2	2.89	32.37	64.74
SN-3	3.74	32.16	64.10

4.1.3. X-ray Diffraction (XRD)

The X- ray diffraction was done by JEOL JDX-II, X-ray diffractometer. The patterns were matched with the standards reference codes by using X per High score plus for the peak matching.

The diffraction peaks appeared at 25.3°, 37.8°, 48.06°, 53.96° and 62.7° for the synthesized catalysts SN-0.1 to SN-3 have their lattice planes (101),(004),(200),(105) and (204) matching with the standard JCPDS Card No.(01-086-1157) which showed that the N-doped TiO_2 has a tetragonal structure with anatase phase.

For the undoped TiO_2 the peaks appeared at 25.3°, 37.8°, 48.03°, 53.89° and 62.6°. They have their lattice planes (101), (004), (200), (105) and (204) matching with the standard JCPDS Card No. (03-065-5714) revealed that the undoped TiO_2 is also tetragonal with anatase phase. Figure 4.16, 4.17 show the stack patterns for all the doped and undoped catalyst

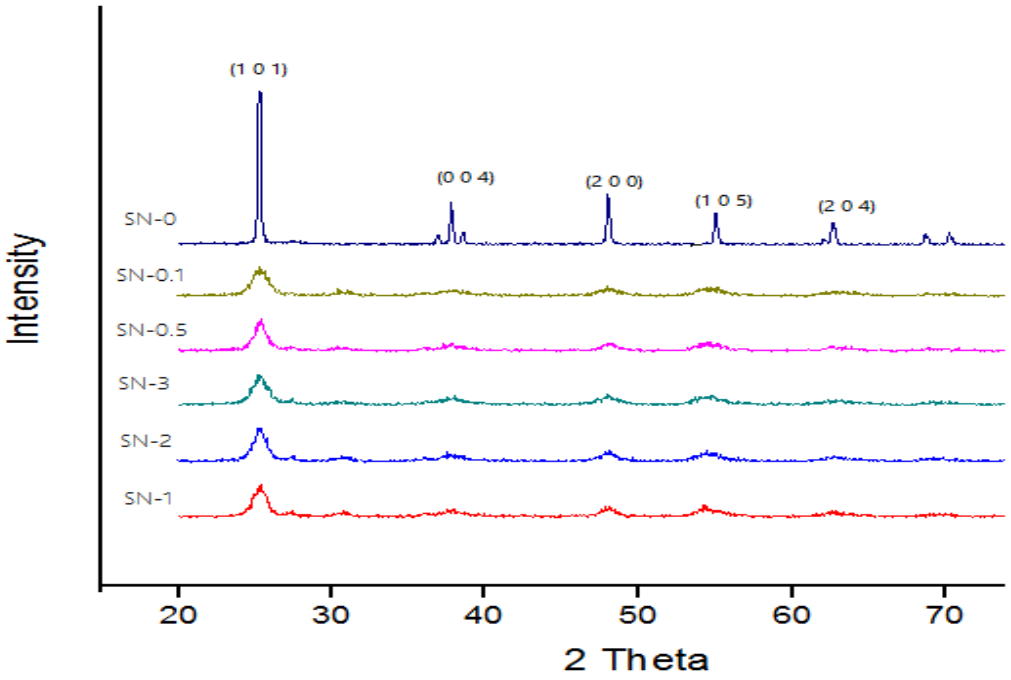

Figure 4.15 XRD Patterns for the synthesized nanocatalysts

The stick patterns for the doped and undoped Titania is shown by the figure 4.15 and 4.16.

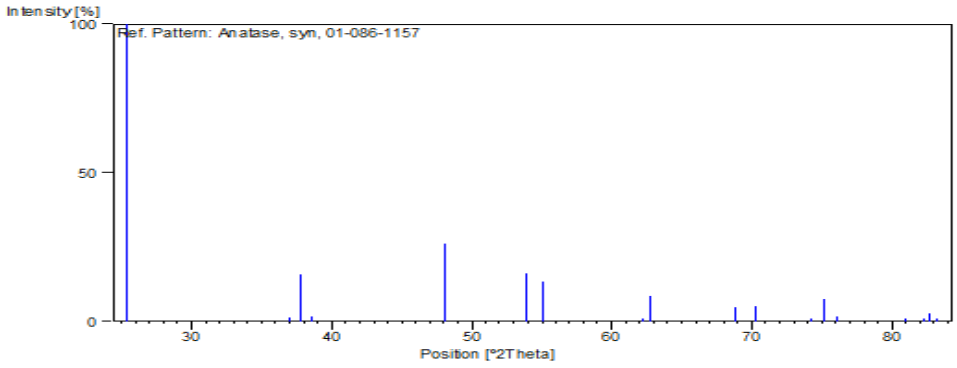

Figure 4.16 Stick pattern of the N-doped TiO_2 nanocatalyst

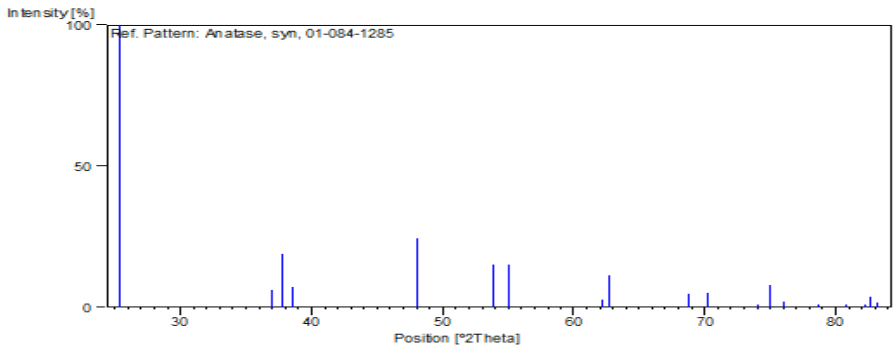

Figure 4.17 Stick pattern of the undoped TiO_2 nanocatalyst

The average crystallite size for all the synthesized catalysts was determined by the Scherer's formula ($D= K\lambda / B\cos\theta$)[59]. The following table shows all the values;

Table 4.2 Crystallite size of as prepared catalyst calculated by Scherer's formula:

Sample code	B observed [2ºTh]	B std [2ºTh]	Peak position [2ºTh]	Crystallite sizes(nm) of the most intense peaks	Average Crystallite size (nm)
SN-1	0.394	0.08	25.3	25.9	**16.5**
	0.63	-	37.8	15.3	
	1.102	-	48.06	8.5	
	0.63	-	53.96	16.2	
SN-2	0.472	-	25.3	20.8	**13.2**
	0.787	-	37.8	11.9	
	0.787	-	48.0	12.3	
	1.26	-	55.06	7.6	
SN-3	0.866	-	25.32	10.4	**12.8**
	1.102	-	37.86	8.2	
	0.394	-	48.06	27.7	
	1.889	-	53.98	4.9	
SN-0.5	0.472	-	25.3	20.8	**13.6**
	0.63	-	37.8	15.3	
	0.787	-	48.10	12.3	
	1.574	-	53.92	6.0	
SN-0.1	0.472	-	25.35	20.8	**10.3**
	1.237	-	37.78	7.3	
	1.102	-	48.07	8.5	
	1.889	-	53.92	4.9	
SN-0	0.157	-	25.3	105.7	**77.3**
	0.197	-	37.8	71.6	
	0.236	-	48.03	55.8	
	0.197	-	53.89	76.3	

4.1.4. Brunauer Emmett-Teller (BET) surface area analysis

BET (Braunauer, Emmett and Teller) was done for the determination of surface area for all the synthesized catalysts. BET analysis was done by Gemini VII 2390 V1.03 (V1.03 t) with nitrogen adsorption analysis. An increase in the surface area is noticed as the size of nanocatalyst is decreased. The surface area of each catalyst synthesized was found from the BET isotherm, plotted between the quantities of nitrogen gas adsorbed and the relative pressure. The pore size and surface area for all the catalysts are shown as follow;

Table 4.3 BET surface area and pore size of the synthesized nanocatalyst and Bulk TiO_2:

Sample code	**BET surface area** (m^2/gm.)	**Pore size (**A^o**)**
bulk TiO_2	10.38	18.44
SN-0	87.89	18.35
SN-0.1	113.65	18.38
SN-0.5	78.81	18.28
SN-1	100.68	18.32
SN-2	115.01	18.42
SN-3	193.04	18.32

Figure 4.18 to 4.24 shows the BET surface area plots for bulk TiO_2, SN-1, SN-2, SN-3, SN-0.5, SN-0.1 and SN-0 nanocatalysts respectively.

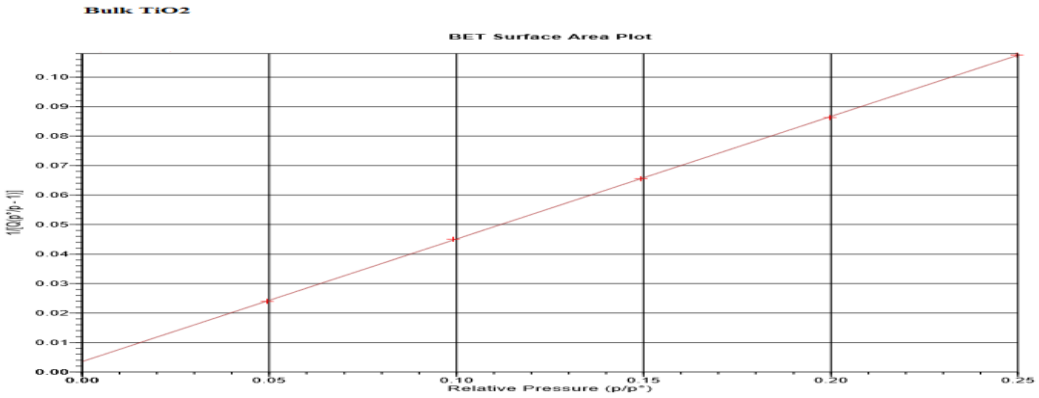

Figure 4.18 BET surface area plot of bulk TiO_2

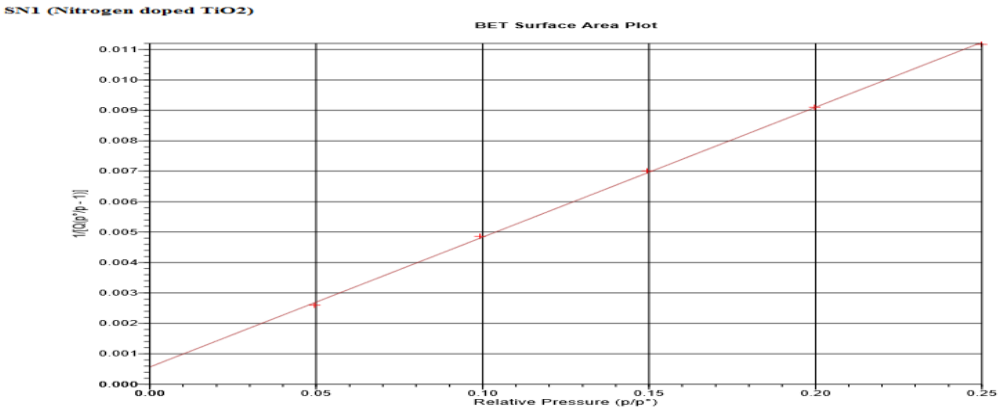

Figure 4.19 BET surface area plot of synthesized N-doped TiO_2 (SN-1)

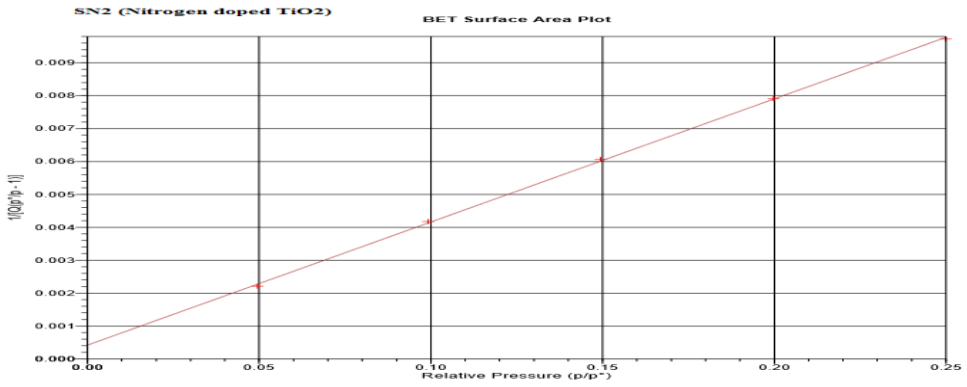

Figure 4.20 BET surface area plot of synthesized N-doped TiO_2 (SN-2)

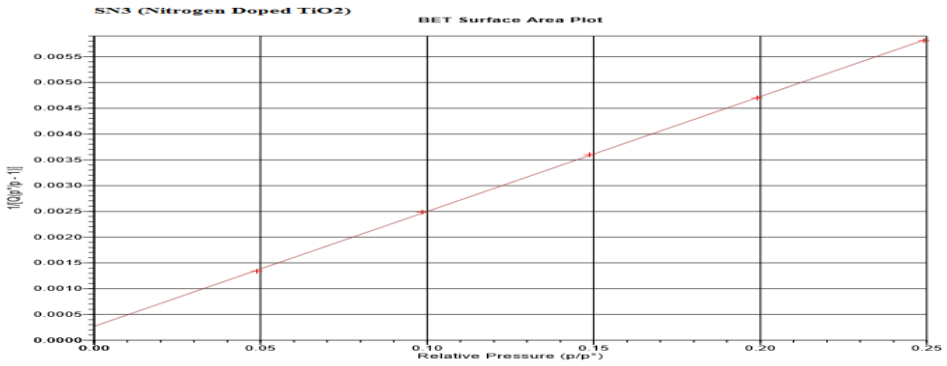

Figure 4.21 BET surface area plot of synthesized N-doped TiO_2 (SN-3)

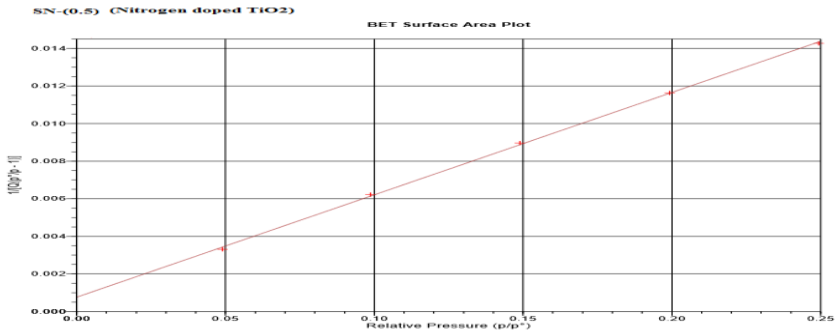

Figure 4.22 BET surface area plot of synthesized N-doped TiO_2 (SN-0.5)

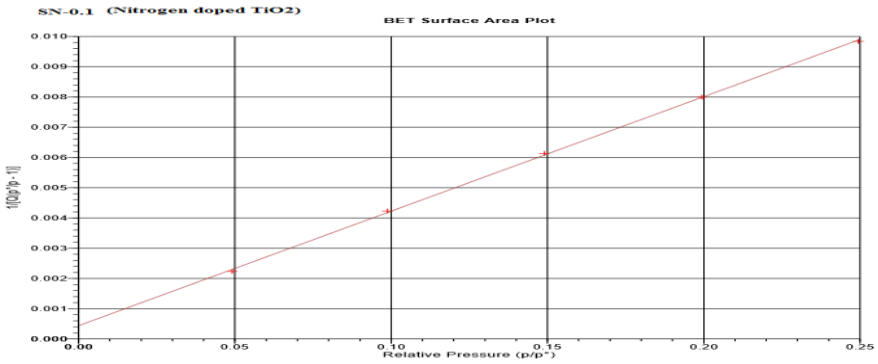

Figure 4.23 BET surface area plot of synthesized N-doped TiO_2 (SN-0.1)

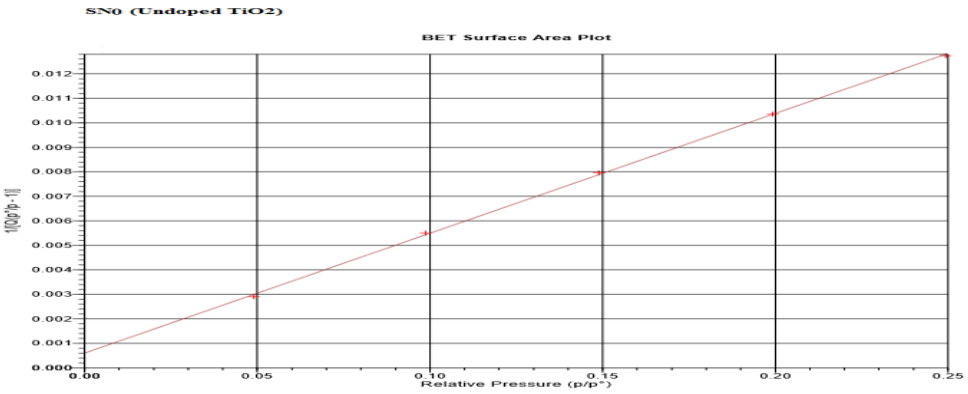

Figure 4.24 BET surface area plot of synthesized Undoped TiO_2 (SN-0)

4.1.5. UV-visible spectrophotometric analysis and band gap measurement

The UV-visible absorption spectra of all the synthesized nanocatalysts and the Bulk TiO_2 were taken by the UV–visible spectrophotometer. Samples were prepared in the form of colloidal solution in methanol and using the quartz cuvette for taking the absorption spectra in the range of 200 nm to 800 nm wavelength. From the absorbance value the band gap of each composition was measured through tauc plot between the hυ(eV) on x- axis and the $(\alpha hf)^{1/2}$ on the y-axis. Lowering of band gap is observed as the Nitrogen content is increased through doping .The band gap of SN-3 has the lowest band gap i-e 2.562 eV and thus has the highest photo catalytic activity.

The band gap for the synthesized nanocatalysts with their maximum lambda is shown as follow;

Table 4.4 Optical band gap of the N-doped and undoped TiO_2:

Catalyst	Band Gap (eV)	Max Lambda
SN-1	2.87	437
SN-2	2.81	441
SN-3	2.56	476
SN-0.5	2.82	442
SN-0.1	2.98	431
SN-0	3.19	230
bulk TiO_2	3.20	225

The UV-vis absorption spectra and Tauc plots for the bulk TiO_2 and as prepared N-doped and undoped nanocatalysts are shown as follow;

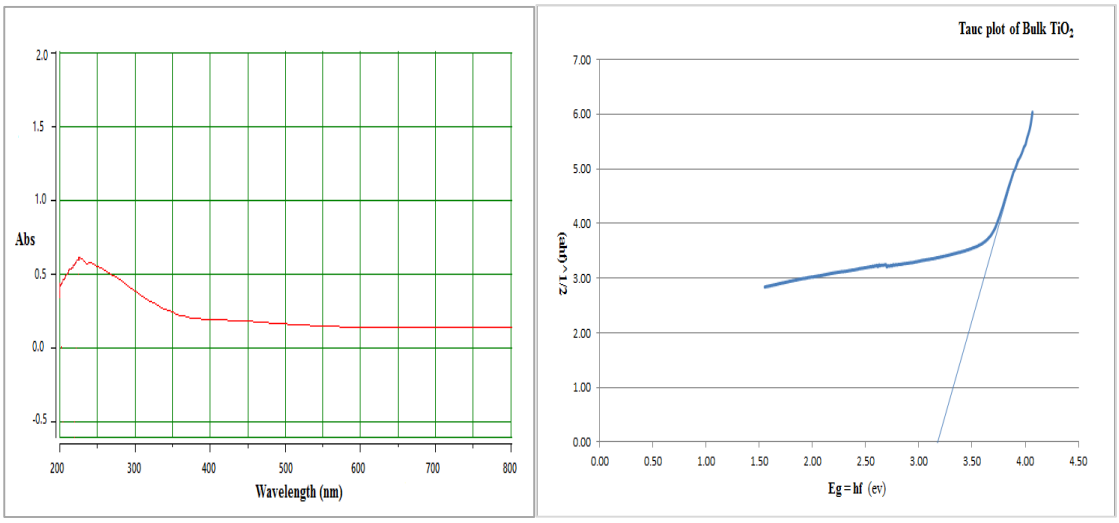

Figure 4.25 UV-vis absorption spectrum of bulk TiO_2 and band gap calculation by Tauc plot

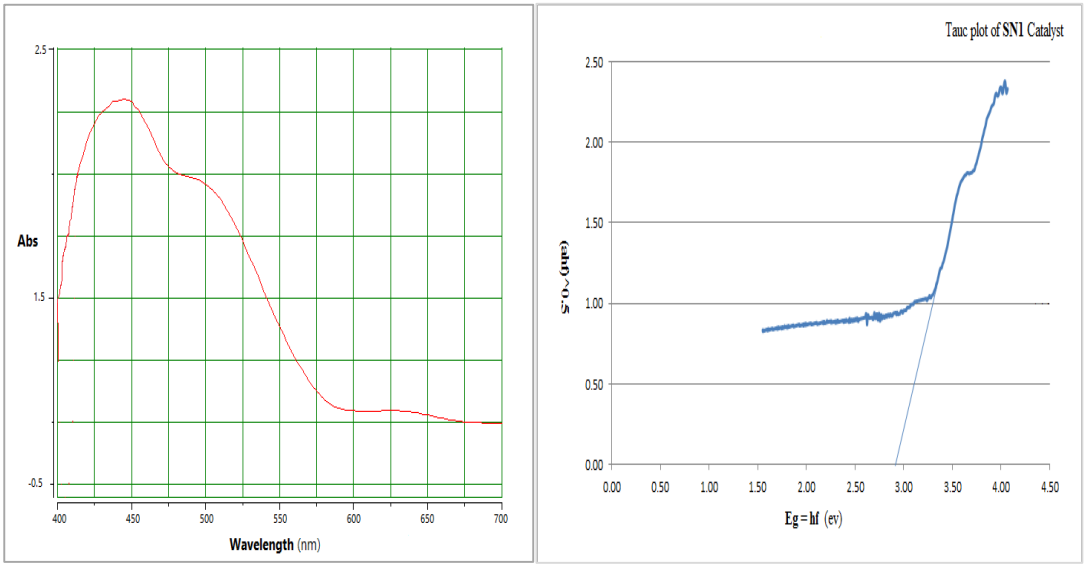

Figure 4.26 UV-vis absorption spectrum of N-doped TiO_2 (SN-1) and the respective Tauc plot

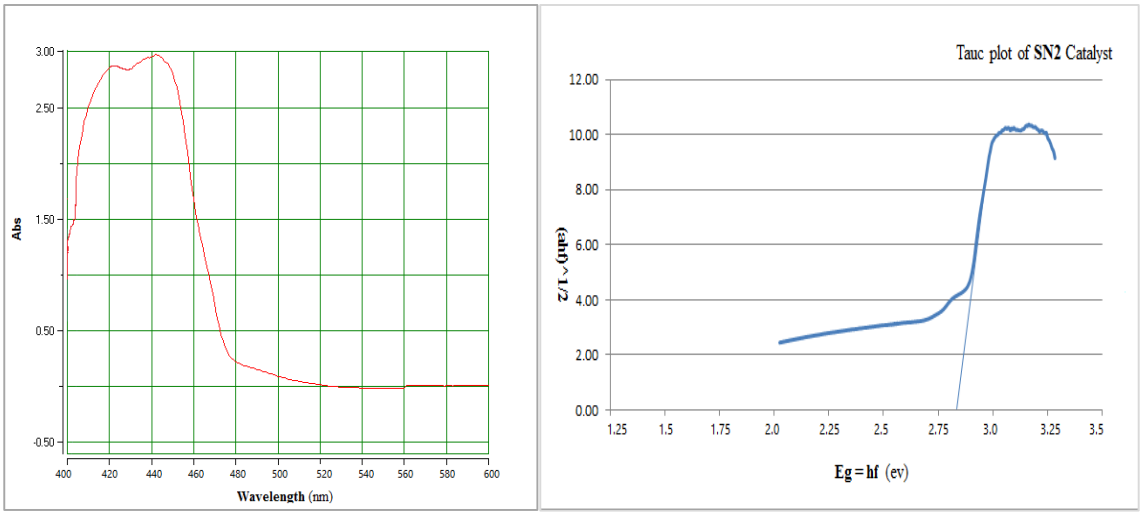

Figure 4.27 UV-vis absorption spectrum of N-doped TiO_2 (SN-2) and the respective Tauc plot

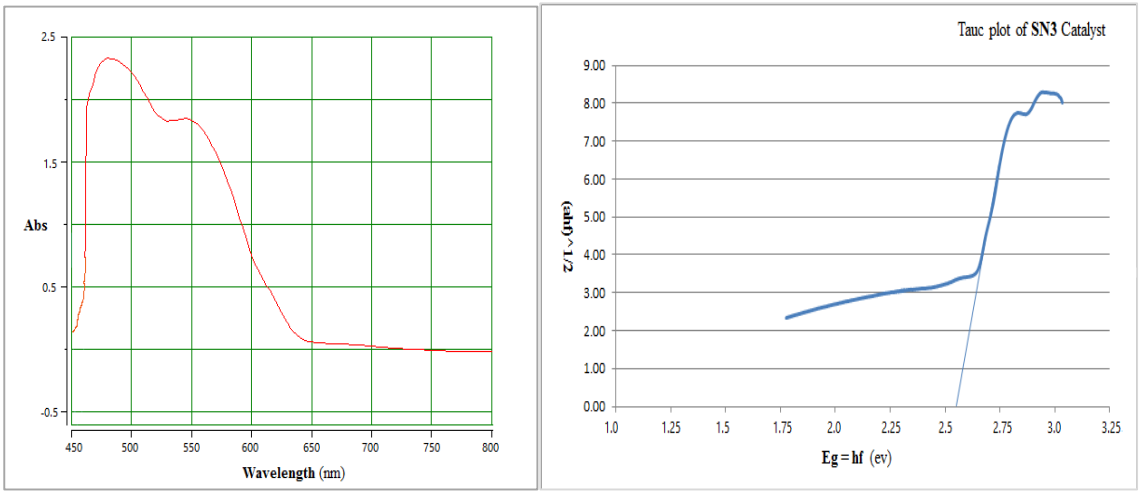

Figure 4.28 UV-vis absorption spectrum of N-doped TiO_2 (SN-3) and the respective Tauc plot

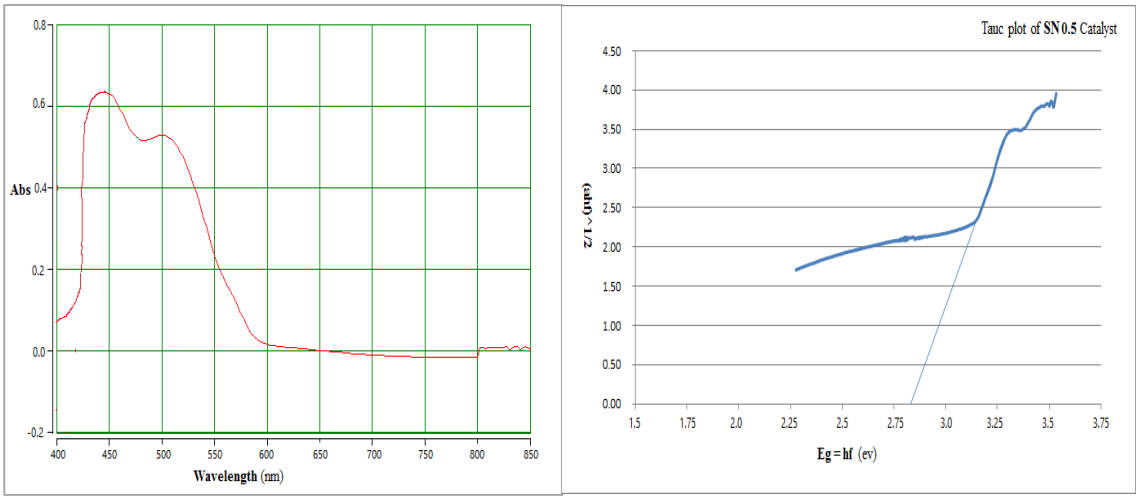

Figure 4.29 UV-vis absorption spectrum of N-doped TiO_2 (SN-0.5) and the respective Tauc plot

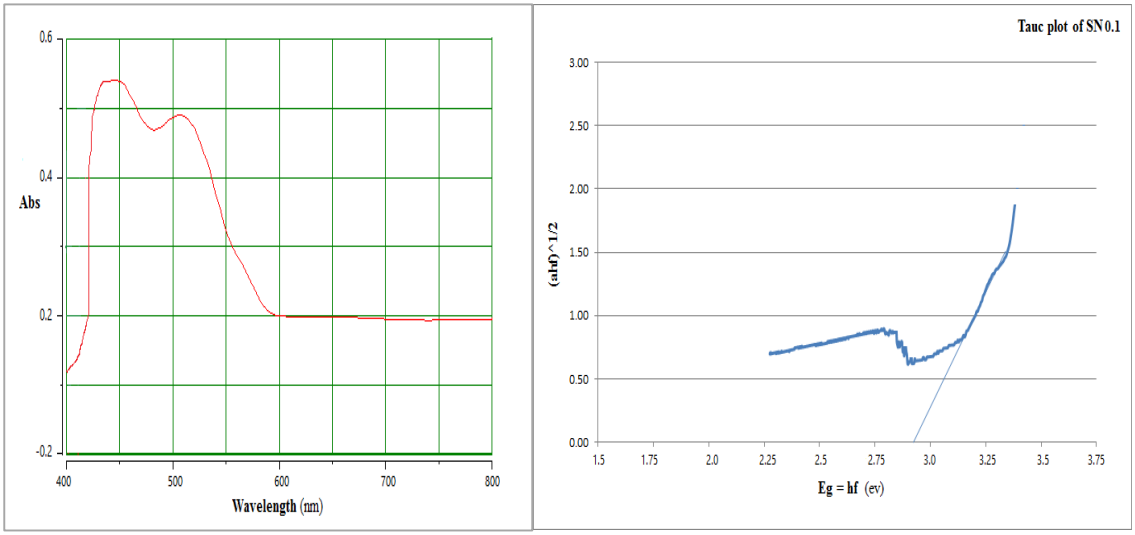

Figure 4.30 UV-vis absorption spectrum of N-doped TiO_2 (SN-0.1) and the respective Tauc plot

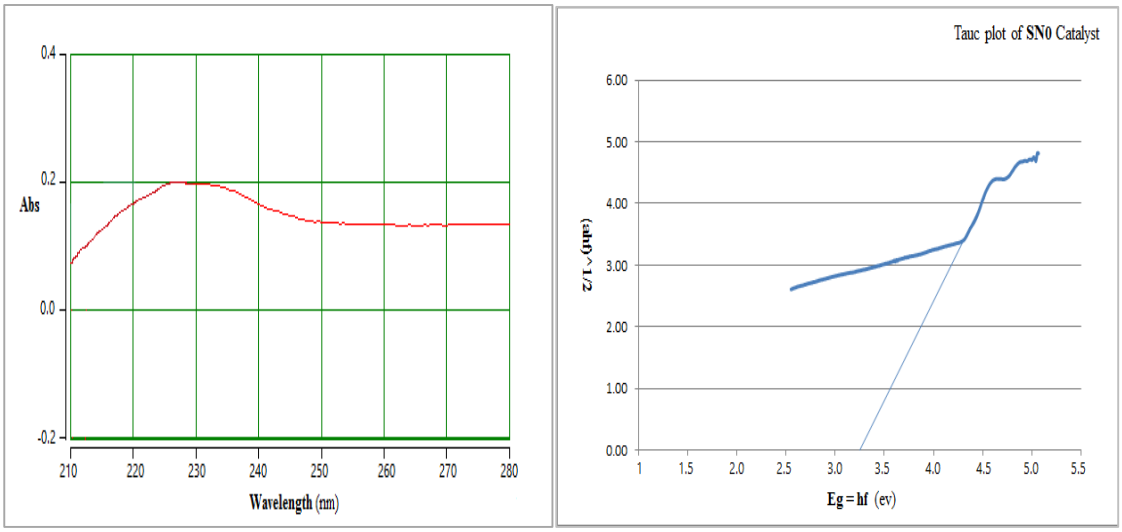

Figure 4.31 UV-vis absorption spectrum of N-doped TiO_2 (SN-0) and the respective Tauc plot

4.2. Investigation of the catalytic activity of the synthesized nanocatalysts against acephate and omethoate:

4.2.1. Degradation experiment

The activity of the as prepared catalysts was evaluated from the degradation studies of pesticides acephate and omethoate.

Pure acephate (Sigma Aldrich (98% purity) was used. A solution of 0.1 mM was prepared in spectroscopic grade methanol as a stock solution; it was diluted to 0.01 mM for further photo catalysis. For the experiment about 50 ml sample was taken in a vial and catalyst was added to this vial (properly capped). The samples were stirred for two hours in dark to ensure adsorption desorption equilibrium. Then the samples was kept in the sunlight and continuously stirred. The experiments were performed at room temperature and neutral pH. At different time interval aliquots were taken and their absorbance was examined from UV-vis spectrophotometer. The decrease in absorbance showed the decrease in acephate concentration.

4.2.1.1. Acephate degradation in dark

Acephate degradation in dark is low as compared to sunlight. Figure 4.32 shows the comparison of catalyst efficiency both in sunlight and dark.

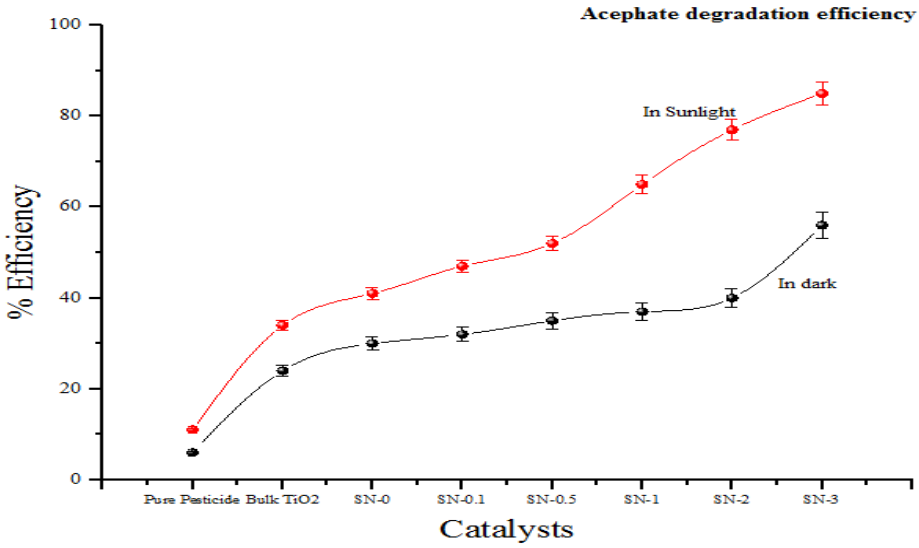

Figure 4.32 Comparison of %efficiencies of all catalyst in sunlight and dark

Each catalyst was separately studied and its activity under sunlight and in dark room was compared. The following figures show the comparison of all catalyst respectively for the degradation of acephate pesticide.

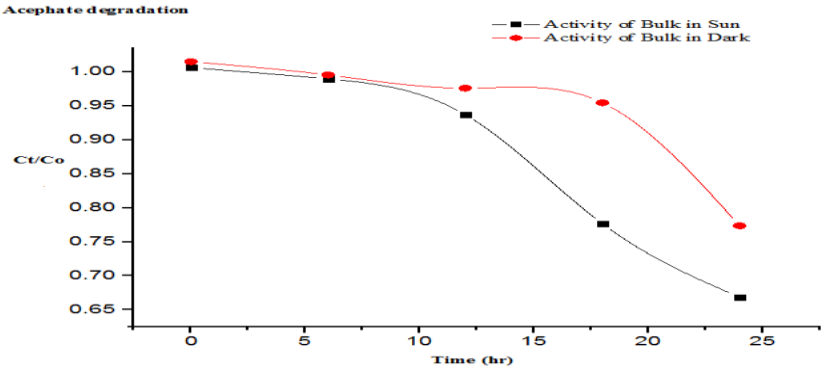

Figure 4.33 Activity of bulk TiO_2 against acephate under sunlight and in dark

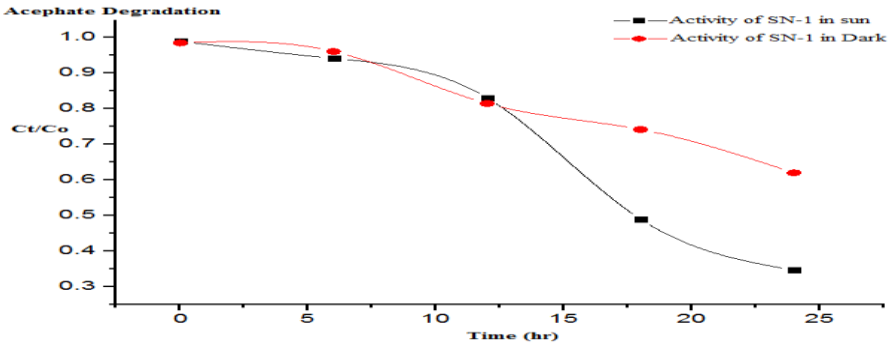

Figure 4.34 Activity of SN-1 against acephate under sunlight and in dark

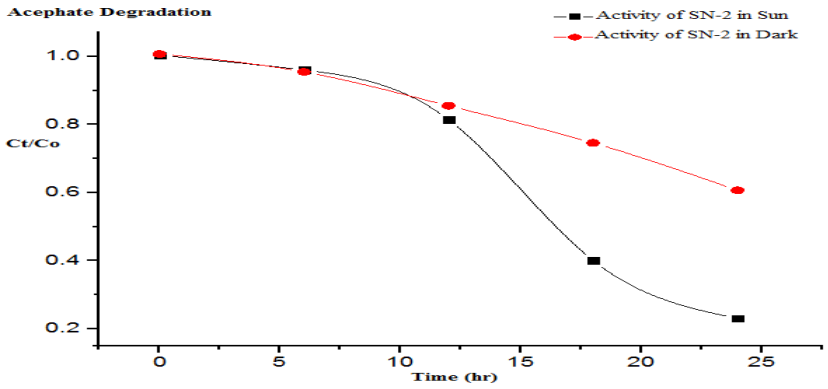

Figure 4.35 Activity of SN-2 against acephate under sunlight and in dark

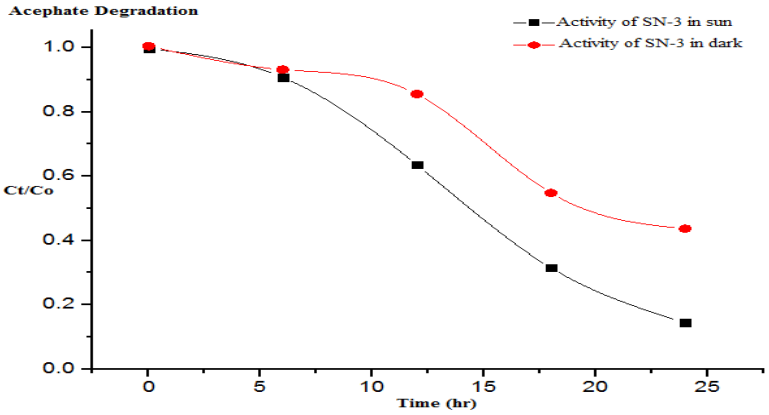

Figure 4.36 Activity of SN-3 against acephate under sunlight and in dark

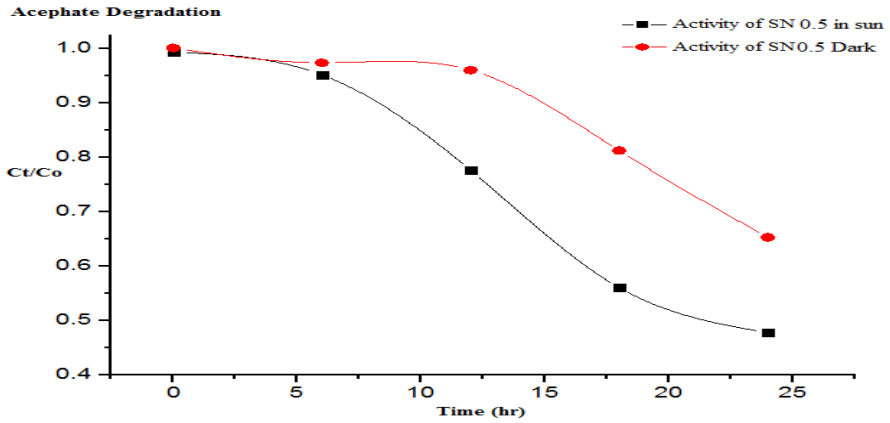

Figure 4.37 Activity of SN-0.5 against acephate under sunlight and in dark

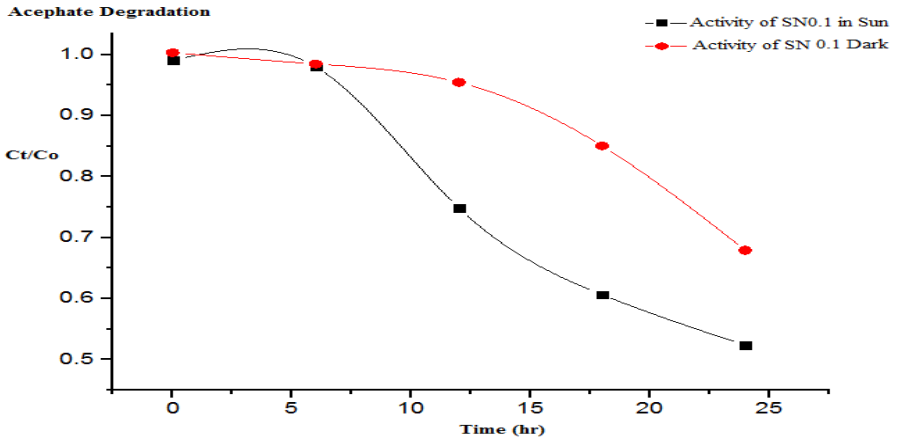

Figure 4.38 Activity of SN-0.1 against acephate under sunlight and in dark

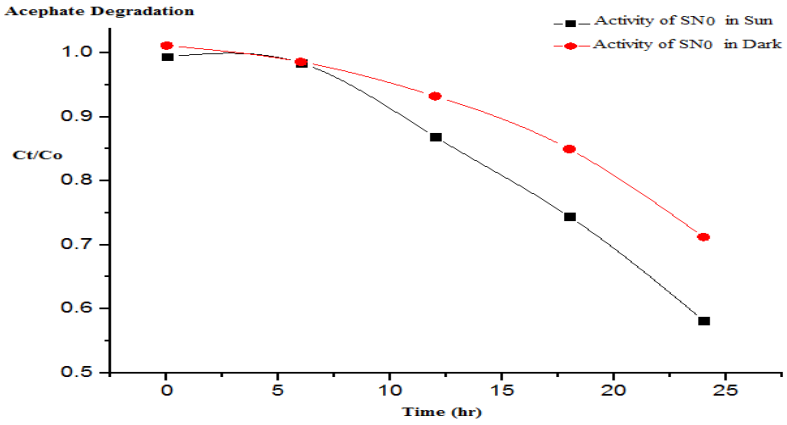

Figure 4.39 Activity of SN-0 against acephate under sunlight and in dark

The catalytic activity of all the catalysts for acephate is given as below;

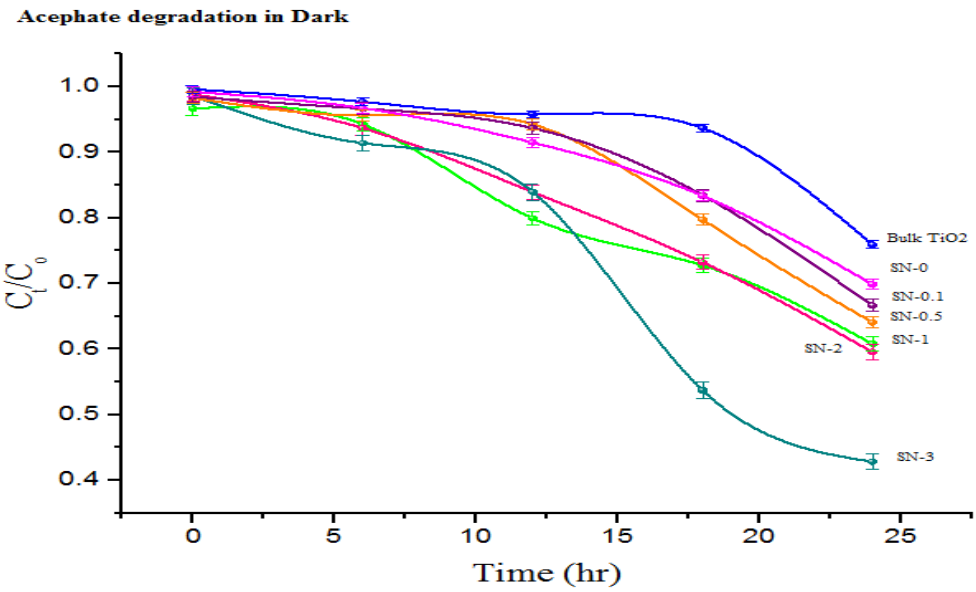

Figure 4.40 Activity of all catalysts against acephate in dark

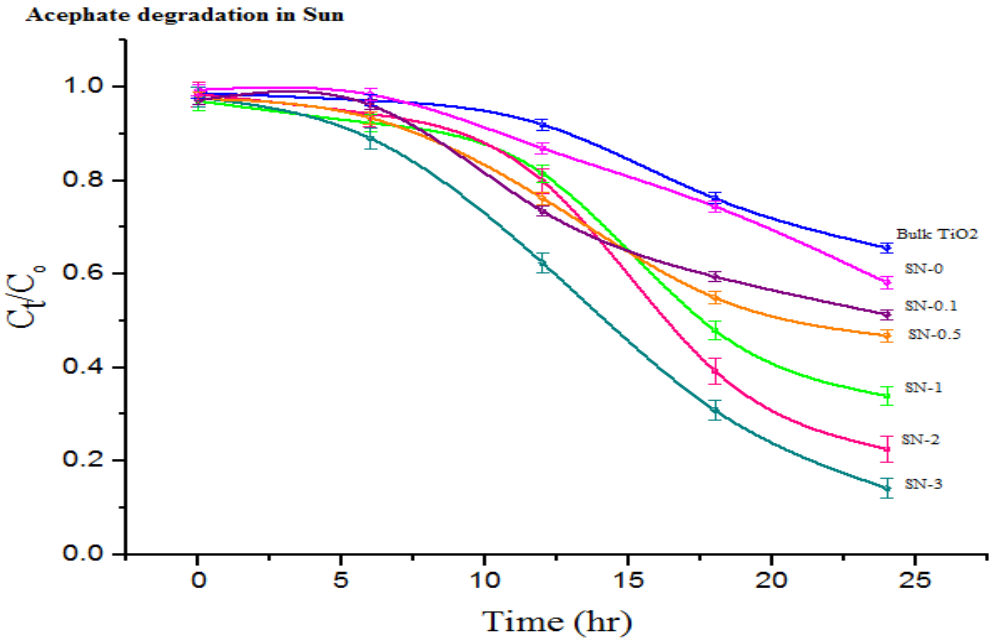

Figure 4.41 Activity of all catalysts against acephate in sunlight

The concentration values were found from the absorbance recorded from the UV-vis spectrophotometer at 205 nm which is the maximum wavelength (λmax) for the acephate pesticide. Table 4.5 shows the findings of degradation of acephate;

Table 4.5 Degradation rate calculation for acephate from the absorbance recorded (In dark)

Catalyst	Time (hr)	Absorbance examined	C_t	C_o	Ct/Co	ln Ct/Co	negative of ln Ct/Co
Bulk TiO_2	0	1.043	0.53	0.53	1.00	0.00	0.00
	6	1.023	0.52		0.98	-0.02	0.02
	12	1.003	0.51		0.96	-0.04	0.04
	18	0.981	0.50		0.94	-0.07	0.07
	24	0.795	0.40		0.76	-0.28	0.28
SN-0	0	1.039	0.53	0.53	0.99	-0.01	0.01
	6	1.013	0.51		0.97	-0.03	0.03
	12	0.958	0.48		0.91	-0.09	0.09
	18	0.873	0.44		0.83	-0.18	0.18
	24	0.732	0.37		0.70	-0.36	0.36
SN-0.1	0	1.031	0.52	0.53	0.98	-0.02	0.02
	6	1.012	0.51		0.97	-0.03	0.03
	12	0.981	0.50		0.94	-0.07	0.07
	18	0.874	0.44		0.83	-0.18	0.18
	24	0.698	0.35		0.67	-0.41	0.41
SN-0.5	0	1.029	0.52	0.53	0.98	-0.02	0.02
	6	1.001	0.51		0.96	-0.05	0.05
	12	0.987	0.50		0.94	-0.06	0.06
	18	0.835	0.42		0.80	-0.23	0.23
	24	0.671	0.34		0.64	-0.45	0.45
SN-1	0	1.012	0.51	0.53	0.97	-0.03	0.03
	6	0.987	0.50		0.94	-0.06	0.06
	12	0.837	0.42		0.80	-0.22	0.22
	18	0.762	0.39		0.73	-0.32	0.32
	24	0.637	0.32		0.61	-0.50	0.50
SN-2	0	1.035	0.52	0.53	0.99	-0.01	0.01
	6	0.981	0.50		0.94	-0.07	0.07
	12	0.879	0.44		0.84	-0.18	0.18
	18	0.767	0.39		0.73	-0.31	0.31
	24	0.624	0.32		0.60	-0.52	0.52
SN-3	0	1.032	0.52	0.53	0.99	-0.01	0.01
	6	0.957	0.48		0.91	-0.09	0.09
	12	0.879	0.44		0.84	-0.18	0.18
	18	0.563	0.28		0.54	-0.62	0.62
	24	0.449	0.23		0.43	-0.85	0.85

All these experiments were performed in triplicates to ensure accuracy of the practical work. The results are shown by table 4.6 and its deviation is also given in the same table.

Table 4.6 Experimental results of all triplicates and its standard deviation (for acephate in dark)

Catalyst	Time (hr)	Ct/Co			Average Ct/Co	Std Dev
		Exp-A	Exp-B	Exp-C		
Bulk TiO_2	0	1.02	1.00	0.98	1.00	± 0.02
	6	1.00	0.98	0.96	0.98	± 0.02
	12	0.97	0.96	0.95	0.96	± 0.01
	18	0.96	0.94	0.92	0.94	± 0.02
	24	0.77	0.76	0.75	0.76	± 0.01
SN-0	0	1.01	0.99	0.97	0.99	± 0.02
	6	1.00	0.97	0.94	0.97	± 0.03
	12	0.92	0.91	0.90	0.91	± 0.01
	18	0.84	0.83	0.82	0.83	± 0.01
	24	0.72	0.7	0.68	0.70	± 0.02
SN-0.1	0	0.99	0.98	0.97	0.98	± 0.01
	6	1.00	0.97	0.94	0.97	± 0.03
	12	0.96	0.94	0.92	0.94	± 0.02
	18	0.86	0.83	0.80	0.83	± 0.03
	24	0.68	0.67	0.66	0.67	± 0.01
SN-0.5	0	1.01	0.98	0.95	0.98	± 0.03
	6	0.98	0.96	0.94	0.96	± 0.02
	12	0.97	0.94	0.91	0.94	± 0.03
	18	0.84	0.8	0.76	0.80	± 0.04
	24	0.65	0.64	0.63	0.64	± 0.01
SN-1	0	0.98	0.97	0.96	0.97	± 0.01
	6	0.96	0.94	0.92	0.94	± 0.02
	12	0.81	0.8	0.79	0.80	± 0.01

	18	0.76	0.73	0.70	0.73	± 0.03
	24	0.63	0.61	0.59	0.61	± 0.02
SN-2	0	1.01	0.99	0.97	0.99	± 0.02
	6	0.96	0.94	0.92	0.94	± 0.02
	12	0.87	0.84	0.81	0.84	± 0.03
	18	0.74	0.73	0.72	0.73	± 0.01
	24	0.62	0.6	0.58	0.60	± 0.02
SN-3	0	1.00	0.99	0.98	0.99	± 0.01
	6	0.93	0.91	0.89	0.91	± 0.02
	12	0.85	0.84	0.83	0.84	± 0.01
	18	0.56	0.54	0.52	0.54	± 0.02
	24	0.44	0.43	0.42	0.43	± 0.01

4.2.1.2. Degradation of acephate in sunlight

The main objective of the study was to investigate the catalytic activity of the as prepared catalyst in presence of visible light (sunlight). So the acephate pesticide was decomposed under sunlight by the same procedure and for accurate results the experiments were performed in triplicates. Table 4.7 and 4.8 shows the results obtained.

Table 4.7 Degradation rate calculation for acephate from the absorbance recorded (in sunlight)

Catalyst	Time (hr)	Absorbance examined	C_t	C_o	Ct/Co (Sun)	ln Ct/Co	negative of ln Ct/Co
Bulk TiO_2	0	1.034	0.52	0.53	0.99	-0.01	0.01
	6	1.017	0.51		0.97	-0.03	0.03
	12	0.963	0.49		0.92	-0.08	0.08
	18	0.798	0.40		0.76	-0.27	0.27
	24	0.687	0.35		0.66	-0.42	0.42
SN-0	0	1.021	0.52	0.53	0.97	-0.03	0.03
	6	1.011	0.51		0.97	-0.04	0.04
	12	0.893	0.45		0.85	-0.16	0.16
	18	0.765	0.39		0.73	-0.31	0.31
	24	0.598	0.30		0.57	-0.56	0.56
SN-0.1	0	1.018	0.52	0.53	0.97	-0.03	0.03
	6	1.007	0.51		0.96	-0.04	0.04
	12	0.769	0.39		0.73	-0.31	0.31

	18	0.623	0.32		0.59	-0.52	0.52
	24	0.538	0.27		0.51	-0.67	0.67
SN-0.5	0	1.021	0.52	0.53	0.97	-0.03	0.03
	6	0.978	0.49		0.93	-0.07	0.07
	12	0.798	0.40		0.76	-0.27	0.27
	18	0.576	0.29		0.55	-0.60	0.60
	24	0.491	0.25		0.47	-0.76	0.76
SN-1	0	1.016	0.51	0.53	0.97	-0.03	0.03
	6	0.967	0.49		0.92	-0.08	0.08
	12	0.853	0.43		0.81	-0.21	0.21
	18	0.503	0.25		0.48	-0.73	0.73
	24	0.356	0.18		0.34	-1.08	1.08
SN-2	0	1.031	0.52	0.53	0.98	-0.02	0.02
	6	0.987	0.50		0.94	-0.06	0.06
	12	0.837	0.42		0.80	-0.22	0.22
	18	0.412	0.21		0.39	-0.93	0.93
	24	0.237	0.12		0.23	-1.49	1.49
SN-3	0	1.024	0.52	0.53	0.98	-0.02	0.02
	6	0.932	0.47		0.89	-0.12	0.12
	12	0.653	0.33		0.62	-0.47	0.47
	18	0.324	0.16		0.31	-1.17	1.17
	24	0.149	0.08		0.14	-1.95	1.95

Table 4.8 Experimental results of all triplicates and its standard deviation (for acephate in sun)

Catalyst	Time (hr)	Ct/Co			Acephate Avg Ct/Co	Std Dev
		Exp-A	Exp-B	Exp-C		
Bulk TiO_2	0	1.00	0.99	0.98	0.99	± 0.01
	6	1.00	0.97	0.94	0.97	± 0.03
	12	0.94	0.92	0.90	0.92	± 0.02
	18	0.79	0.76	0.73	0.76	± 0.03
	24	0.68	0.66	0.64	0.66	± 0.02
SN-0	0	1.01	0.97	0.93	0.97	± 0.04
	6	1.00	0.97	0.94	0.97	± 0.03
	12	0.87	0.85	0.83	0.85	± 0.02
	18	0.74	0.73	0.72	0.73	± 0.01
	24	0.59	0.57	0.55	0.57	± 0.02
SN-0.1	0	0.99	0.97	0.95	0.97	± 0.02
	6	0.99	0.96	0.93	0.96	± 0.03
	12	0.75	0.73	0.71	0.73	± 0.02

	18	0.61	0.59	0.57	0.59	± 0.02
	24	0.55	0.51	0.47	0.51	± 0.04
SN-0.5	0	1.00	0.97	0.94	0.97	± 0.03
	6	0.97	0.93	0.89	0.93	± 0.04
	12	0.79	0.76	0.73	0.76	± 0.03
	18	0.56	0.55	0.54	0.55	± 0.01
	24	0.49	0.47	0.45	0.47	± 0.02
SN-1	0	0.99	0.97	0.95	0.97	± 0.02
	6	0.93	0.92	0.91	0.92	± 0.01
	12	0.85	0.81	0.77	0.81	± 0.04
	18	0.50	0.48	0.46	0.48	± 0.02
	24	0.38	0.34	0.30	0.34	± 0.04
SN-2	0	0.99	0.98	0.97	0.98	± 0.01
	6	0.97	0.94	0.91	0.94	± 0.03
	12	0.82	0.8	0.78	0.80	± 0.02
	18	0.41	0.39	0.37	0.39	± 0.02
	24	0.26	0.23	0.20	0.23	± 0.03
SN-3	0	0.99	0.98	0.97	0.98	± 0.01
	6	0.93	0.89	0.85	0.89	± 0.04
	12	0.63	0.62	0.61	0.62	± 0.01
	18	0.34	0.31	0.28	0.31	± 0.03
	24	0.15	0.14	0.13	0.14	± 0.01

4.2.1.3. Degradation of omethoate in dark

Same procedure was followed for the omethoate. Omethoate (mol.wt = 213.19 g/mol) was used. A solution of 0.01 mM in spectroscopic grade methanol was used. The decomposition efficiency of all the catalysts was evaluated in absence of light and under sunlight. Figure 4.42 shows the % efficiency of all the catalyst in sun and dark;

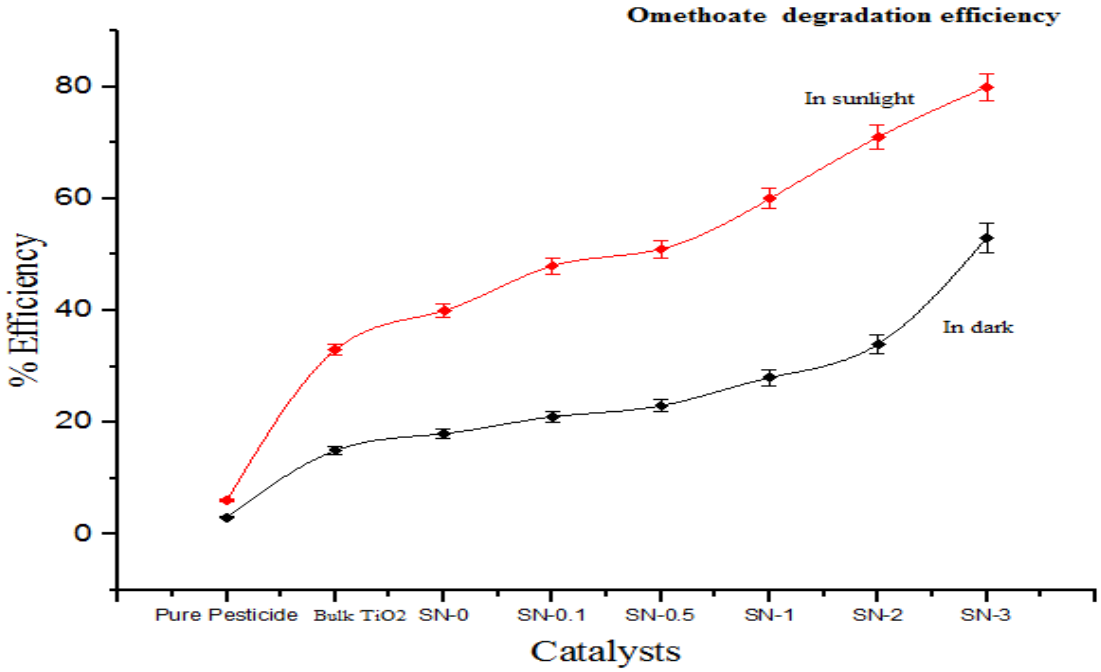

Figure 4.42 Omethoate degradation efficiency in dark and sunlight

For omethoate the comparison of activity in dark and sunlight for each catalyst is given by the following figures;

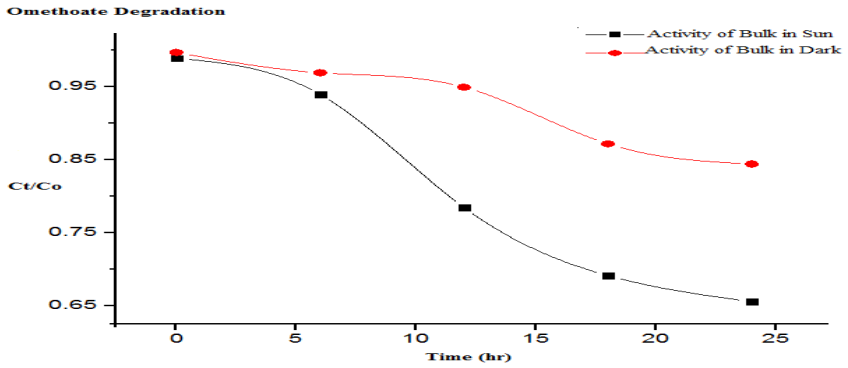

Figure 4.43 Activity of bulk TiO_2 against omethoate pesticide (In dark and sunlight)

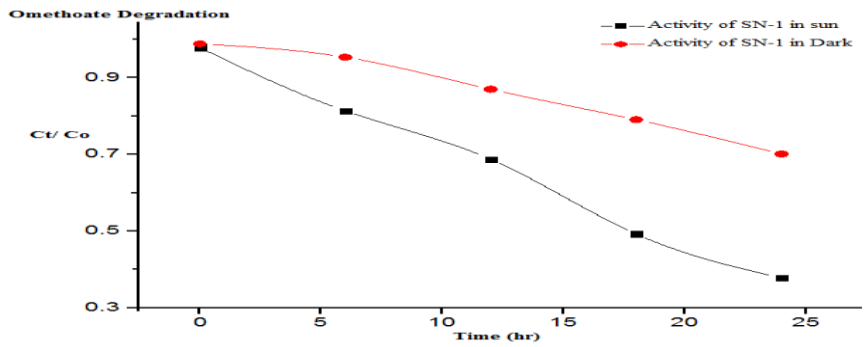

Figure 4.44 Activity of SN-1 against omethoate pesticide (in dark and sunlight)

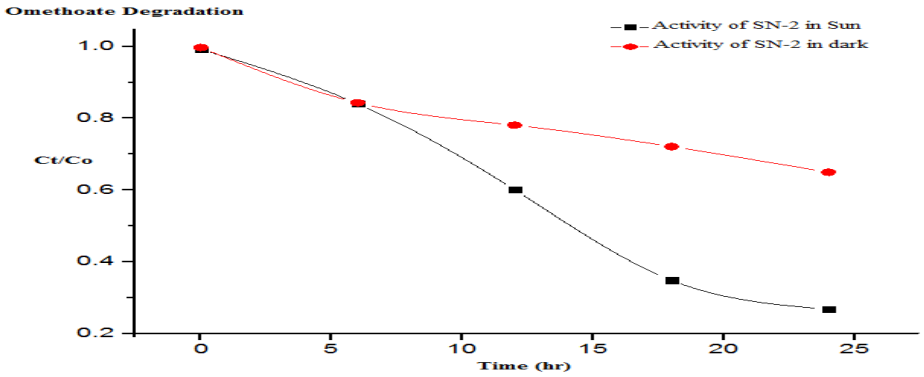

Figure 4.45 Activity of SN-2 against omethoate pesticide (In dark and sunlight)

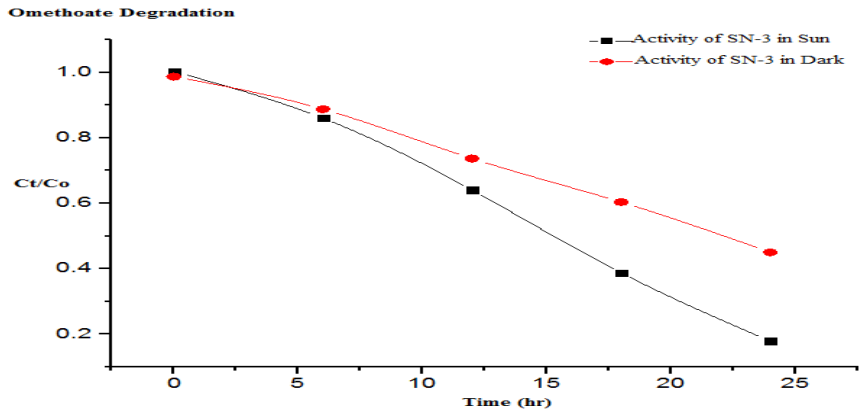

Figure 4.46 Activity of SN-3 against omethoate pesticide (In dark and sunlight)

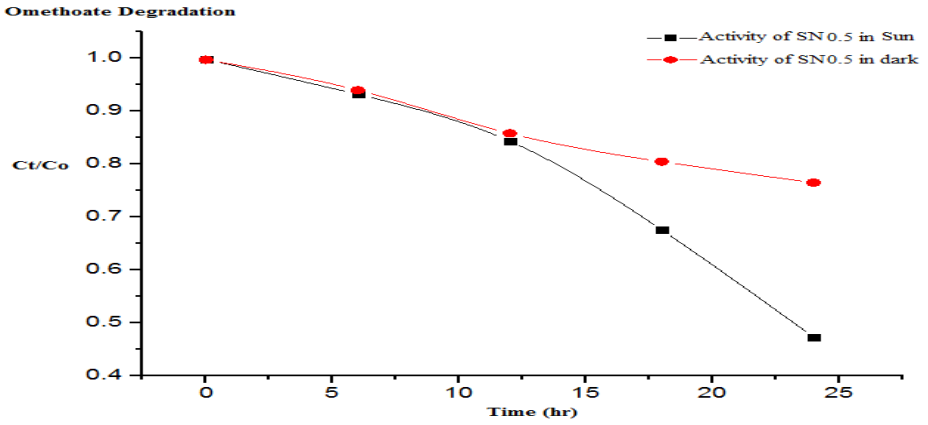

Figure 4.47 Activity of SN-0.5against omethoate pesticide (in dark and sunlight)

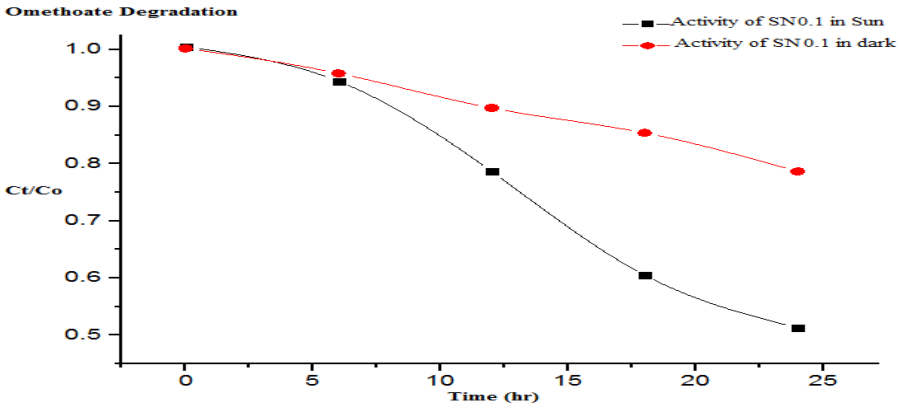

Figure 4.48 Activity of SN-0.1 against omethoate pesticide (in dark and sunlight)

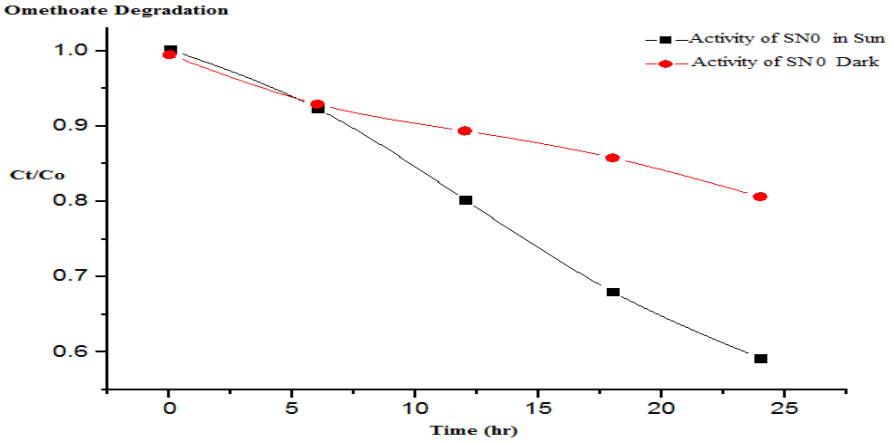

Figure 4.49 Activity of SN-0 against omethoate pesticide (in dark and sunlight)

The catalytic activity of all catalysts is shown in the following figure with the error;

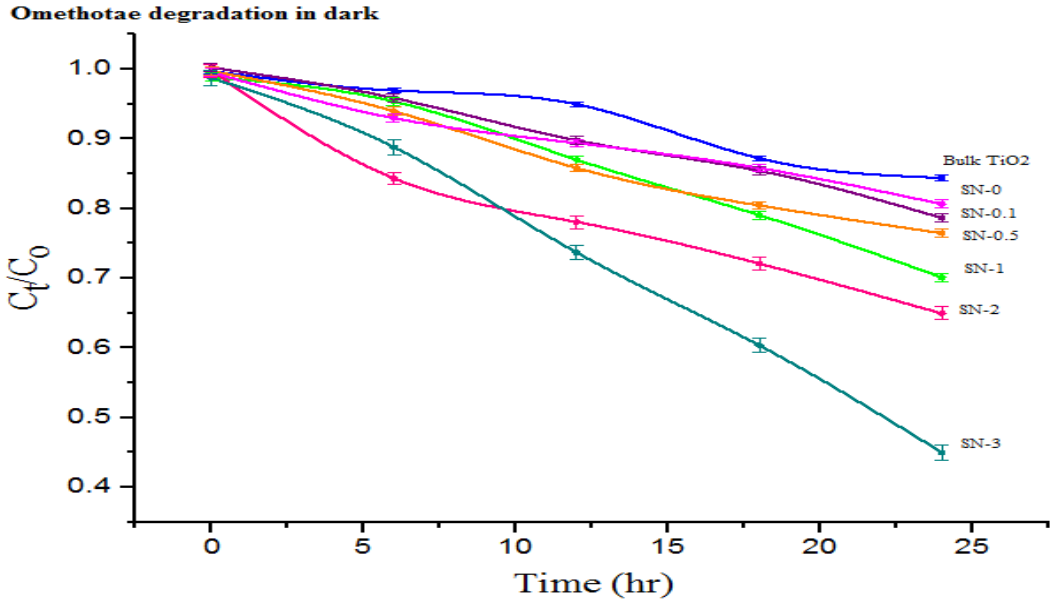

Figure 4.50 Activity of all catalysts against omethoate pesticide in dark

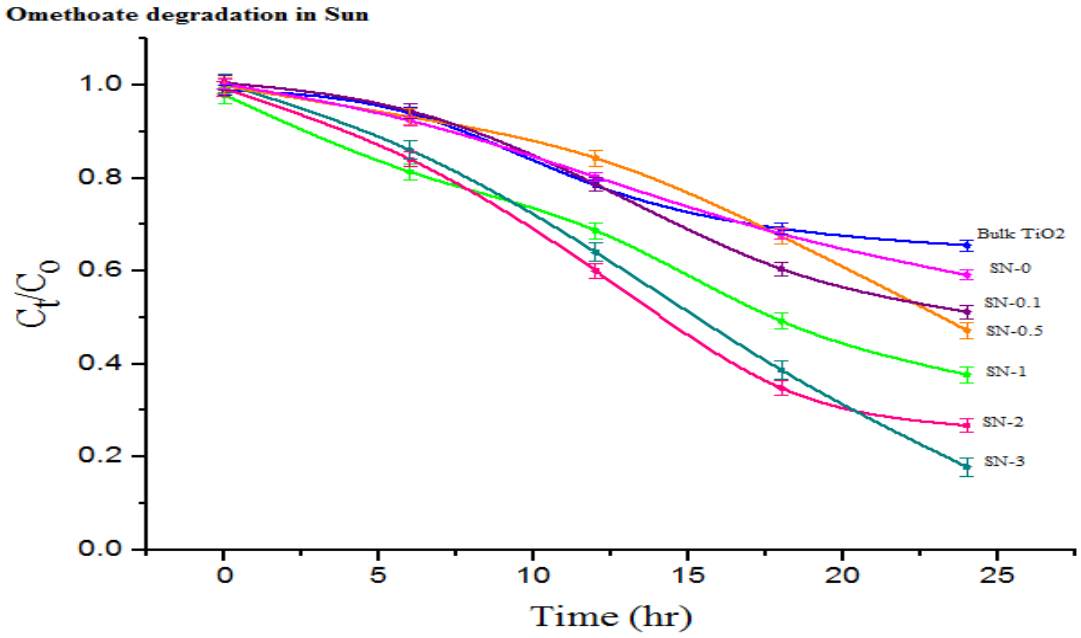

Figure 4.51 Activity of all catalysts against omethoate pesticide in sunlight

The concentration values for omethoate at different time interval were found from the absorbance data recorded from at 207 nm which is the maximum wavelength (λmax) for the pesticide. The following table shows the values;

Table 4.9 Degradation rate calculation for omethoate from the absorbance (in dark)

Catalyst	Time (hr)	Absorbance Dark	C_t	C_o	Ct/Co (Dark)	ln Ct/Co	negative of ln Ct/Co
Bulk TiO_2	0	1.031	0.53	0.53	1.00	-0.003	0.003
	6	1.003	0.51		0.97	-0.031	0.031
	12	0.983	0.50		0.95	-0.052	0.052
	18	0.905	0.46		0.87	-0.137	0.137
	24	0.877	0.45		0.84	-0.169	0.169
SN-1	0	1.022	0.52	0.53	0.99	-0.012	0.012
	6	0.987	0.51		0.95	-0.048	0.048
	12	0.903	0.46		0.87	-0.139	0.139
	18	0.823	0.42		0.79	-0.235	0.235
	24	0.733	0.37		0.70	-0.355	0.355
SN-2	0	1.031	0.53	0.53	1.00	-0.003	0.003
	6	0.876	0.45		0.84	-0.171	0.171
	12	0.813	0.41		0.78	-0.248	0.248
	18	0.753	0.38		0.72	-0.327	0.327
	24	0.681	0.34		0.65	-0.432	0.432
SN-3	0	1.021	0.52	0.53	0.99	-0.013	0.013
	6	0.921	0.47		0.89	-0.119	0.119
	12	0.769	0.39		0.74	-0.305	0.305
	18	0.635	0.32		0.60	-0.505	0.505
	24	0.478	0.24		0.45	-0.803	0.803
SN-0.5	0	1.031	0.53	0.53	1.00	-0.003	0.003
	6	0.973	0.50		0.94	-0.062	0.062
	12	0.891	0.45		0.86	-0.153	0.153
	18	0.837	0.43		0.80	-0.218	0.218
	24	0.797	0.41		0.76	-0.268	0.268
SN-0.1	0	1.036	0.53	0.53	1.00	0.002	-0.002
	6	0.992	0.51		0.96	-0.043	0.043
	12	0.931	0.48		0.90	-0.108	0.108
	18	0.887	0.45		0.85	-0.158	0.158
	24	0.819	0.42		0.79	-0.240	0.240
SN-0	0	1.029	0.53	0.53	1.00	-0.005	0.005
	6	0.963	0.49		0.93	-0.073	0.073
	12	0.927	0.47		0.89	-0.112	0.112

	18	0.891	0.45		0.86	-0.153	0.153
	24	0.839	0.43		0.81	-0.215	0.215

Results for triplicate calculated are given as follow (in Table 4.10) with standard deviation;

Table 4.10 Results of omethoate degradation with their standard deviations

Catalyst	Time (hr)	Ct/Co			Omethoate Avg Ct/Co	Std Dev
		Exp-A	Exp-B	Exp-C		
Bulk TiO_2	0	1.01	1.00	0.99	1.00	± 0.010
	6	0.98	0.97	0.96	0.97	± 0.010
	12	0.98	0.95	0.92	0.95	± 0.030
	18	0.89	0.87	0.85	0.87	± 0.020
	24	0.86	0.84	0.82	0.84	± 0.020
SN-1	0	1.01	0.99	0.97	0.99	± 0.020
	6	0.96	0.95	0.94	0.95	± 0.010
	12	0.89	0.87	0.85	0.87	± 0.020
	18	0.82	0.79	0.76	0.79	± 0.030
	24	0.71	0.70	0.69	0.70	± 0.010
SN-2	0	1.03	1.00	0.97	1.00	± 0.030
	6	0.86	0.84	0.82	0.84	± 0.020
	12	0.79	0.78	0.77	0.78	± 0.010
	18	0.74	0.72	0.7	0.72	± 0.020
	24	0.67	0.65	0.63	0.65	± 0.020
SN-3	0	1.01	0.99	0.97	0.99	± 0.020
	6	0.9	0.89	0.88	0.89	± 0.010
	12	0.76	0.74	0.72	0.74	± 0.020
	18	0.61	0.60	0.59	0.60	± 0.010
	24	0.48	0.45	0.42	0.45	± 0.030
SN-0.5	0	1.03	1.00	0.97	1.00	± 0.030
	6	0.99	0.94	0.89	0.94	± 0.050
	12	0.87	0.86	0.85	0.86	± 0.010
	18	0.82	0.80	0.78	0.80	± 0.020
	24	0.77	0.76	0.75	0.76	± 0.010
SN-0.1	0	1.02	1.00	0.98	1.00	± 0.020
	6	0.98	0.96	0.94	0.96	± 0.020
	12	0.91	0.90	0.89	0.90	± 0.010
	18	0.86	0.85	0.84	0.85	± 0.010
	24	0.81	0.79	0.77	0.79	± 0.020

SN-0	0	1.03	1.00	0.97	1.00	± 0.030
	6	0.95	0.93	0.91	0.93	± 0.020
	12	0.91	0.89	0.87	0.89	± 0.020
	18	0.87	0.86	0.85	0.86	± 0.010
	24	0.82	0.81	0.8	0.81	± 0.010

4.2.1.4. Degradation of omethoate in sunlight

Omethoate was decomposed by the as prepared catalyst under sunlight as well. The efficiency and comparison of activity was shown by the above figures as mentioned. The numerical values for the all the experiments are shown by the following tables;

Table 4.11 Degradation of omethoate in sunlight

Catalyst	Time (hr)	Absorbance Sunlight	C_t	C_o	Ct/Co (Sun)	ln Ct/Co	negative of ln Ct/Co
bulk TiO_2	0	1.023	0.52	0.53	0.99	-0.011	0.011
	6	0.973	0.50		0.94	-0.062	0.062
	12	0.817	0.42		0.78	-0.243	0.243
	18	0.723	0.37		0.69	-0.369	0.369
	24	0.687	0.35		0.66	-0.422	0.422
SN-1	0	1.012	0.52	0.53	0.98	-0.022	0.022
	6	0.846	0.43		0.81	-0.207	0.207
	12	0.719	0.36		0.69	-0.375	0.375
	18	0.523	0.26		0.49	-0.708	0.708
	24	0.407	0.20		0.38	-0.975	0.975
SN-2	0	1.026	0.53	0.53	0.99	-0.008	0.008
	6	0.873	0.45		0.84	-0.174	0.174
	12	0.632	0.32		0.60	-0.510	0.510
	18	0.378	0.18		0.35	-1.054	1.054
	24	0.297	0.14		0.27	-1.316	1.316
SN-3	0	1.037	0.53	0.53	1.00	0.003	-0.003
	6	0.893	0.46		0.86	-0.151	0.151
	12	0.672	0.34		0.64	-0.445	0.445
	18	0.417	0.21		0.39	-0.949	0.949
	24	0.207	0.09		0.18	-1.722	1.722
SN-0.5	0	1.032	0.53	0.53	1.00	-0.002	0.002
	6	0.965	0.49		0.93	-0.071	0.071
	12	0.876	0.45		0.84	-0.171	0.171

	18	0.707	0.36		0.68	-0.393	0.393
	24	0.503	0.25		0.47	-0.749	0.749
SN-0.1	0	1.039	0.53	0.53	1.00	0.005	-0.005
	6	0.978	0.50		0.94	-0.057	0.057
	12	0.819	0.42		0.79	-0.240	0.240
	18	0.636	0.32		0.60	-0.503	0.503
	24	0.543	0.27		0.51	-0.669	0.669
SN-0	0	1.036	0.53	0.53	1.00	0.002	-0.002
	6	0.957	0.49		0.92	-0.080	0.080
	12	0.835	0.43		0.80	-0.220	0.220
	18	0.712	0.36		0.68	-0.385	0.385
	24	0.623	0.31		0.59	-0.524	0.524

Table 4.12 Omethoate degradation results of repeated experiments and their deviation

Catalyst	Time (hr)	Ct/Co			Omethoate Avg Ct/Co	Std Dev
		Exp-A	Exp-B	Exp-C		
bulk TiO_2	0	1.01	0.99	0.97	0.99	± 0.020
	6	0.98	0.94	0.9	0.94	± 0.040
	12	0.79	0.78	0.77	0.78	± 0.010
	18	0.71	0.69	0.67	0.69	± 0.020
	24	0.69	0.66	0.63	0.66	± 0.030
SN-1	0	1.01	0.98	0.95	0.98	± 0.030
	6	0.83	0.81	0.79	0.81	± 0.020
	12	0.71	0.69	0.67	0.69	± 0.020
	18	0.51	0.49	0.47	0.49	± 0.020
	24	0.39	0.38	0.37	0.38	± 0.010
SN-2	0	1.02	0.99	0.96	0.99	± 0.030
	6	0.86	0.84	0.82	0.84	± 0.020
	12	0.63	0.60	0.57	0.60	± 0.030
	18	0.37	0.35	0.33	0.35	± 0.020
	24	0.28	0.27	0.26	0.27	± 0.010
SN-3	0	1.01	1.00	0.99	1.00	± 0.010
	6	0.88	0.86	0.84	0.86	± 0.020
	12	0.67	0.64	0.61	0.64	± 0.030
	18	0.43	0.39	0.35	0.39	± 0.040
	24	0.21	0.18	0.15	0.18	± 0.030
SN-0.5	0	1.03	1.00	0.97	1.00	± 0.030
	6	0.99	0.93	0.89	0.94	± 0.050
	12	0.86	0.84	0.82	0.84	± 0.020
	18	0.71	0.68	0.65	0.68	± 0.030

	24	0.49	0.47	0.45	0.47	± 0.020
SN-0.1	0	1.01	1.00	0.99	1.00	± 0.010
	6	0.96	0.94	0.92	0.94	± 0.020
	12	0.82	0.79	0.76	0.79	± 0.030
	18	0.62	0.60	0.58	0.60	± 0.020
	24	0.54	0.51	0.48	0.51	± 0.030
SN-0	0	1.02	1.00	0.98	1.00	± 0.020
	6	0.93	0.92	0.91	0.92	± 0.010
	12	0.83	0.80	0.77	0.80	± 0.030
	18	0.71	0.68	0.65	0.68	± 0.030
	24	0.6	0.59	0.58	0.59	± 0.010

The reaction kinetics for the photo catalytic reaction can be estimated from the following reaction;

$$-r \text{ pesticide} = kC_{cat}{}^{a}C^{b}$$

where Ccat is the concentration of catalyst, "a" is reaction order with respect to the catalyst and C is the concentration of pesticide, and "b" is the reaction order with respect to the pesticide.

As the concentration of catalyst is constant so the expression can be simplified to;

$$-r \text{ pesticide} = KC^{b} \qquad \text{(where } K = kC_{cat}\text{)}$$

So dCt/dt can be written as $\ln Ct/Co = -Kt$

For finding the order of reaction for acephate and omethoate degradation a plot between ln Co/Ct vs time is given by the following figures;

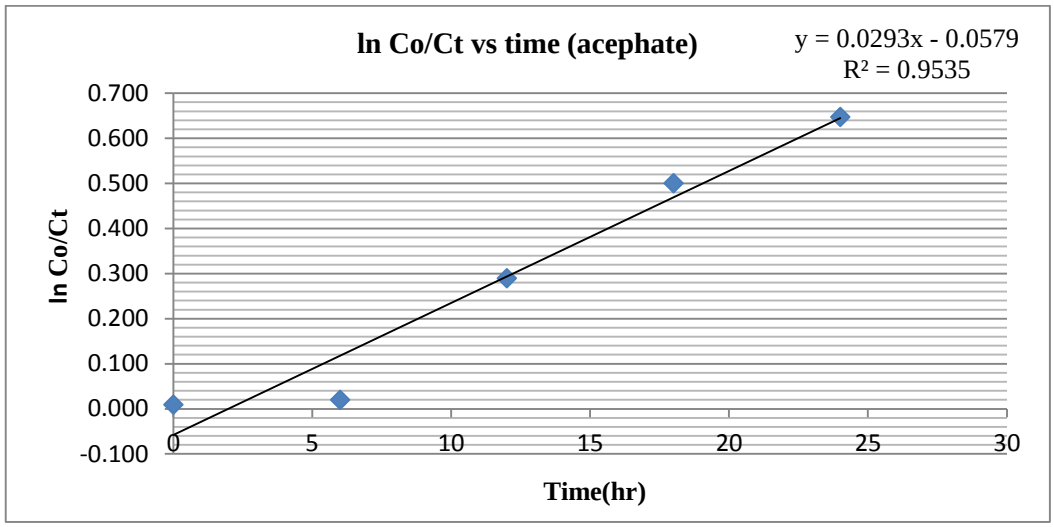

Figure 4.52 Plot between ln Co/Ct vs time (acephate)

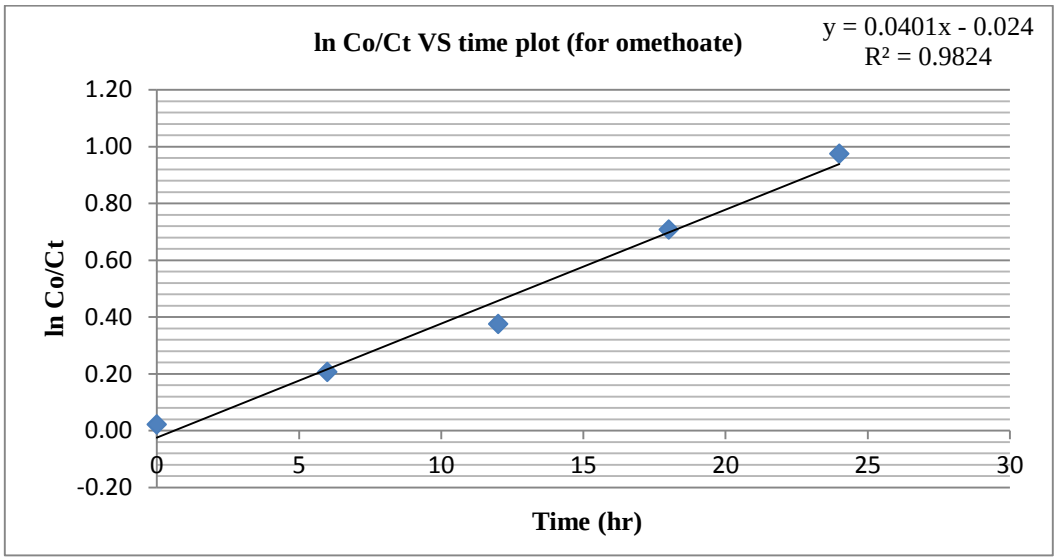

Figure 4.53 Plot between ln Co/Ct vs time (omethoate)

The linearity of graph shows the order of reaction is first order under pseudo condition. The rate constant can be calculated from the slope of the graph.

Chapter: 5 Conclusions

Nitrogen doped TiO_2 nanoparticles were synthesized efficiently from sol-gel method. Different ratios of urea added gave different Nitrogen loading. All the catalysts were then characterized by SEM, XRD, UV visible Spectroscopy and BET.

The synthesized nanoparticles were spherical in morphology as investigated through scanning electron microscopy. The crystal sizes given by XRD confirm the particles in nano range. The surface area per mass of the catalyzed was increases as shown by the BET.

The bang gap was calculated by Tauc Plot, the plots show the variation occurred in band gap of the N-doped TiO_2 nanocatalysts as compared to the band gap of TiO_2. A decrease in band gap i-e red shift was observed after nitrogen loading.

Among all the catalyst synthesized SN-3 (1:3) was found to be the most active because of smaller size, lager surface area and lower band gap.

The activities of all the catalysts were studied against acephate and omethoate pesticides. The efficiency of SN-3 was the highest among all.

The efficiency of synthesized catalyst was also compared with the bulk TiO_2.

References:

[1] M. Z. Faridi, *Pak. J. Commer. Soc. Sci.* **2012**, *6*, 133-146.

[2] E. R. De Ong, *Soil Science* **1956**, *82*, 344.

[3] F. P. Garcia, S. Y. C. Ascencio, John C. Gaytan Oyarzun, A. C. Hernandez, P. V. Alavarado, *Environmental Science and Toxicology* **2012**, *1*, 279-293.

[4] D. Benedetti, F. R. Da Silva, K. Kvitko, S. P. Fernandes, J. da, **2014**.

[5] E. Downing, in *Environmental Monitoring and Pest Management, Vol. CA 95814-3510* (Ed.: D. o. P. Regulation), Sacramento, **2000**.

[6] Z. Qiang, W. Ling, F. Tian, *Chemosphere* **2013**, *90*, 1966-1972.

[7] H. J. Kim, C. J. Lee, M. R. Karim, M. S. Kim, M. S. Lee, *Spectrochimica acta. Part A, Molecular and biomolecular spectroscopy* **2011**, *78*, 179-184.

[8] M. Ashraf, M. Öztürk, M. S. A. Ahmad, A. Aksoy, *Crop Production for Agricultural Improvement*, Springer Dordrecht Heidelberg new york london, **2012**.

[9] M. D. Joel Fuhrman, in *Diseaseproof*, New York **2009**.

[10] D. Tilman, *Proc. Natl. Acad. Sci. USA* **1999**, *96* 5995– 6000.

[11] E. C. Oerke, H. W. Dehne, *Crop Protection* **2004**, *23*, 275-285.

[12] M. W. Aktar, D. Sengupta, A. Chowdhury, *Interdiscip Toxicol* **2009**, *2*, 1-12.

[13] J. P. G. Webster, R. G. Bowles, N. T. Williams, *Crop Protection* **1999**, *18*, 83-89.

[14] V. R. Diware, M. Husain, S. K. Dahiwelkar, *International Journal of Emerging Trends in Engineering and Development* **2014**, *3*.

[15] W. H. Organization, **2011**.

[16] R. J. Gimello, T. Fields, in *Historic Pesticide Contamination Task Force* (Ed.: D. o. E. P. N. Jersey), Robert C. Shinn, Commissioner, New Jersey **1999**.

[17] M. Salehi, H. Hashemipour, M. Mirzaee, *American Journal of Environmental Engineering* **2012**, *2*, 1-7.

[18] K. L. D. Henderson, J. B. Belden, S. Zhao, J. R. Coats, *Zeitschrift für Naturforschung C* **2005**, *61*.

[19] V. Polshettiwar, R. S. Varma, *Green Chemistry* **2010**, *12*, 743.

[20] X. Hong, Z. Wang, W. Cai, F. Lu, J. Zhang, Y. Yang, N. Ma, Y. Liu, *Chem. Mater.* **2005**, *17*, 1548-1552.

[21] C. H. Bartholomew, R. J. Farrauto, *Fundamentals of Industrial Catalytic Process*, Clarendon Press. Oxford, **2006**.

[22] A. Fujishima, X. Zhang, *Comptes Rendus Chimie* **2006**, *9*, 750-760.

[23] R. Asahi, T. Morikawa, H. Irie, T. Ohwaki, *Chemical reviews* **2014**, *114*, 9824-9852.

[24] S. Chaturvedi, P. N. Dave, N. K. Shah, *Journal of Saudi Chemical Society* **2012**, *16*, 307-325.

[25] M. Pelaez, N. T. Nolan, S. C. Pillai, M. K. Seery, P. Falaras, A. G. Kontos, P. S. M. Dunlop, J. W. J. Hamilton, J. A. Byrne, K. O'Shea, M. H. Entezari, D. D. Dionysiou, *Applied Catalysis B: Environmental* **2012**, *125*, 331-349.

[26] W. Choi, A. Termin, M. R. Hoffmann, *The Journal of Physical Chemistry* **1994**, *98*, 13669-13679.

[27] C.-C. Wang, Z. Zhang, J. Y. Ying, *Nanostructured Materials* **1997**, *9*, 583-586.

[28] L. Cao, A. Huang, F.-J. Spiess, S. L. Suib, *Journal of Catalysis* **1999** *188*, 48-57.

[29] A. K. Sharma, R. K. Tiwari, M. S. Gaur, *Arabian Journal of Chemistry* **2012**.

[30] G. C. Lakshmi;, S. Ananda;, R. Somashekar;, C. Ranganathaiah;, *International Journal of NanoScience and Nanotechnology* **2012**, *3*, 47-63.

[31] A. H. Abdullah, L. K. Mun, Z. Zainal, M. Z. Hussein, *International Journal of Chemistry* **2013**, *5*.

[32] C. Jin, J. Li, J. Wang, S. Han, Z. Wang, Q. Sun, *Journal of Nanomaterials* **2014**, *2014*, 1-7.

[33] S. Chen, Y. Liu, *Chemosphere* **2007**, *67*, 1010-1017.

[34] J. Santhanalakshmi, R. Komalavalli, P. Venkatesan, *Nanoscience and Nanotechnology* **2012**, *2*, 8-12.

[35] T. Rojviroon, A. Laobuthee, S. Sirivithayapakorn, *International Journal of Photoenergy* **2012**, *2012*, 1-8.

[36] P. Namkhang, W. J. An, W. N. Wang, K. S. Rane, P. Kongkachuichay, P. Biswas, *J Nanosci Nanotechnol* **2013**, *13*, 2376-2381.

[37] R. Khan, T. J. Kim, *Journal of hazardous materials* **2009**, *163*, 1179-1184.

[38] Y. Ma, J. Zhang, B. Tian, F. Chen, L. Wang, *Journal of hazardous materials* **2010**, *182*, 386-393.

[39] Y. Zhang, Z.-R. Tang, X. Fu, Y.-J. Xu, *Applied Catalysis B: Environmental* **2011**, *106*, 445-452.

[40] F. Wang, K. Zhang, *Journal of Molecular Catalysis A: Chemical* **2011**, *345*, 101-107.

[41] J. Virkutyte, V. Jegatheesan, R. S. Varma, *Bioresour Technol* **2012**, *113*, 288-293.

[42] S. T. Martin;, C. L. Morrison;, M. R. Hoffman;, *J. Phys. Chem.* **1994**, *98*, 13695-13704

[43] J. Choi, H. Park, *J. Phys. Chem. C* **2010**, *114*, 783–792.

[44] V. B. R. Boppana, R. F. Lobo, *Journal of Catalysis* **2011**, *281*, 156-168.

[45] K. B. Jaimy, S. Ghosh, S. Sankar, K. G. K. Warrier, *Materials Research Bulletin* **2011**, *46*, 914-921.

[46] T. Siva Rao, T. A. Segne, T. Susmitha, A. Balaram Kiran, C. Subrahmanyam, *Advances in Materials Science and Engineering* **2012**, *2012*, 1-9.

[47] J. Ananpattarachai, P. Kajitvichyanukul, S. Seraphin, *Journal of hazardous materials* **2009**, *168*, 253-261.

[48] P. Anil Kumar Reddy, P. Venkata Laxma Reddy, V. Maitrey Sharma, B. Srinivas, V. D. Kumari, M. Subrahmanyam, *Journal of Water Resource and Protection* **2010**, *02*, 235-244.

[49] X.-K. Wang, C. Wang, W.-L. Guo, J.-G. Wang, *Materials Research Bulletin* **2011**, *46*, 2041-2044.

[50] H. Diker, C. Varlikli, K. Mizrak, A. Dana, *Energy* **2011**, *36*, 1243-1254.

[51] P. V. R. K. Ramacharyulu, J. Praveen Kumar, G. K. Prasad, B. Sreedhar, *Materials Chemistry and Physics* **2014**, *148*, 692-698.

[52] C. C. C. C. D. of, R. Pesticide Regulation, California. pp. 108–163, **1972**, 108–163.

[53] G. R. Echavia, F. Matzusawa, N. Negishi, *Chemosphere* **2009**, *76*, 595-600.

[54] W. Fu, Y. Wang, C. He, J. Zhao, *Journal of Advanced Oxidation Technologies* **2012**, *15*, 177-182.

[55] X. Zhang, J. Zhou, Y. Gu, D. Fan, *Journal of Nanomaterials* **2015**, 1-6.

[56] Z. Xiu-Feng, M. Xian-Feng, Z. Zhi-Hong, L. Lang, J. Dian-Zeng, *Journal of Inorganic Materials* **2004**, *19*, 140-146.

[57] T. Yugui, W. Yaoming, Y. Shilei, Y. Lianbin, *International Biodeterioration & Biodegradation* **2008**, *62*, 239-243.

[58] Z. di-shun, W. Jia-lei, Z. Xue-heng, Z. Juan, *Chem. Res. Chinese Universities* **2009**, *25*, 543-549

[59] G. SC, T. C, D. J., in *The 1st ECTI Annual Conference*, Pattaya Thailand, **2004**, pp. 145-148.